RESEARCH MEMORANDUM

for the

Bureau of Aeronautics, Department of the Navy

INVESTIGATION OF STAGE PERFORMANCE OF X24C-2 TEN-STAGE AXIAL-FLOW COMPRESSOR AT DESIGN SPEED

By Harold B. Finger, Leo Cohen
and Warner L. Stewart

Lewis Flight Propulsion Laboratory
Cleveland, Ohio

NATIONAL ADVISORY COMMITTEE
FOR AERONAUTICS
WASHINGTON

NATIONAL ADVISORY COMMITTEE FOR AERONAUTICS

RESEARCH MEMORANDUM

for the

Bureau of Aeronautics, Department of the Navy

INVESTIGATION OF STAGE PERFORMANCE OF X24C-2 TEN-STAGE AXIAL-FLOW COMPRESSOR AT DESIGN SPEED

By Harold B. Finger, Leo Cohen
and Warner L. Stewart

SUMMARY

As part of the program to determine the performance of the X24C-2 ten-stage axial-flow compressor, the stage performance of the unit was investigated at design speed with an inlet-air pressure of 12 inches of mercury absolute and ambient temperature at weight flows corresponding to those of the maximum weight-flow, peak-efficiency, and surge points. The performance of each stage was determined from the total-pressure and temperature distributions measured in each stator-blade row.

A large radial gradient in stage total-pressure ratio was set up in the first stage so that near the surge operating point the stage pressure ratio varied from slightly less than 1.00 at the hub to 1.20 near the tip, giving an average value of approximately 1.10 for the stage. The gradient of pressure ratio was reduced in the second stage and the average pressure ratio was approximately 1.13 at the surge point. With the exception of the fourth stage, the radial gradient of pressure ratio was reversed in all of the remaining stages with an average value of approximately 1.15 so that the gradient of total pressure set up in the first stage was gradually reduced to almost a constant total pressure at the compressor outlet. In the fourth stage, the pressure ratio was practically constant at all radii with an average stage pressure ratio of 1.15 at the surge point. The high turnings required at the hub sections of the third, fourth, and fifth stages in order to compensate for the low turnings at the hub of the first two stages appeared to have caused a region of thick boundary layer with possible separation and backflow to develop in these three intermediate stages.

The comparison of the calculated and measured wall static pressures after the last three stationary-blade rows indicated the gradual build-up in blade wakes and wall boundary layers as the flow passed through these blade rows. The data indicated that at the exit from the outlet guide vanes the effective flow area was approximately 25 percent less than the geometrical annulus area as a result of the effect of the blade wakes and wall boundary layers in blocking the flow area.

For the present compressor, the radial distribution of tangential velocity in each stage was such that the conditions of a symmetrical velocity diagram were being approached at almost all sections.

INTRODUCTION

At the request of the Bureau of Aeronautics, Department of the Navy, the NACA Lewis laboratory conducted an investigation to determine the performance characteristics of the X24C-2 ten-stage axial-flow compressor. The final phase of the investigation relating to the evaluation of the stage performance of the compressor is discussed herein. The over-all performance of the unit over a complete speed range at an inlet-air pressure of 21 inches of mercury absolute and ambient inlet-air temperature is presented in reference 1. The effect of inlet-air pressure and temperature on the over-all performance and the factors affecting the surge characteristics of the compressor are presented in references 2 and 3, respectively.

The previously reported work on this compressor has been limited principally to the over-all performance of the unit. Because a complete evaluation and study of compressor performance requires a knowledge of the detailed flow conditions in each blade row of each stage of the compressor, total-pressure and temperature instrumentation was installed in each stator row. The compressor stage performance as determined from these measurements of total pressures and temperatures is therefore presented herein. Space and time limitations and consideration of the effect of the instrumentation on compressor performance made it necessary to limit the amount of instrumentation used to that essential for determination of stage performance, and to restrict the instrumentation to a type that would not seriously affect compressor performance. During the investigation, the compressor was operated at design speed with an inlet-air pressure of 12 inches of mercury absolute and ambient inlet-air temperature with equivalent air weight flows corresponding to those of the maximum weight-flow, peak-efficiency, and surge points. The stage performance is presented in terms of the measured stage pressure ratios and the calculated velocity diagrams.

[redacted]

The velocities after each blade row were determined by the method of reference 4 from the measured total pressures and temperatures and the relative flow angles. The flow angles out of the inlet guide vanes were determined from the investigation of reference 5. The relative flow angles out of all other blade rows were determined from the rule of Carter and Hughes (reference 6).

APPARATUS AND INSTRUMENTATION

Apparatus

The compressor used in the present investigation was designed to handle an air weight flow of 54.6 pounds per second and to develop a pressure ratio of 4 at 12,000 rpm when operating at sea-level inlet conditions. The compressor consisted of three major components: the inlet section, the stator casing, and the rotor. The blading consisted of a row of inlet guide vanes, 10 rows of rotor blades, 10 rows of stator blades, and a row of outlet guide vanes. A more complete description of the compressor, including construction details and blade data, is presented in reference 1. In addition to the blade data presented in reference 1, the radial distributions of blade camber angle and blade inlet angle are presented in figures 1 and 2, respectively, to give an indication of the blade configuration. The camber angle is defined as the angle between the tangents to the camber line at the leading and trailing edges of the airfoil. The blade inlet angle is the angle between the tangent to the camber line at the leading edge of the airfoil section and the compressor axis. (All symbols used in the figures are defined in the appendix.)

The compressor was driven by a 9000-horsepower variable frequency induction motor through a step-up gearbox. The air passed through a measuring orifice and a butterfly control valve in the inlet ducting into the screened depression tank before entering the compressor. A wooden bellmouth nozzle was fitted into the depression tank to insure smooth air entry into the compressor. The air was discharged from the compressor into a collector, which was connected to the laboratory altitude-exhaust facilities through two discharge ducts. During the present investigation, the compressor could not be insulated to minimize heat transfer between the working fluid and the ambient air because of the large number of instruments installed in the unit. The effect of this change in setup is indicated in the data obtained. A more detailed description of the setup is given in reference 1.

Instrumentation

The air weight flow through the compressor was measured by a calibrated, submerged adjustable orifice located in a straight section of the inlet ducting. The conditions of the air entering and leaving the compressor were determined from the measurements described in reference 1 and were made in accordance with the standard procedures outlined in reference 7. In addition, measurements of static pressures at the outer wall of the annular flow passage were taken before and after each blade row as an indication of static-pressure rise through the compressor.

The interstage instrumentation installed specifically for this investigation consisted of three total-pressure rakes and three total-temperature rakes (fig. 3) located midway between adjacent stator blades and midway along the blade chord in each stator row. The three temperature rakes and the three pressure rakes were located approximately 120° apart circumferentially. Each rake contained three radial measuring stations, which were located at the area centers of equal elements of annular area.

The total-pressure rake (fig. 3(a)) was made up of three tubes having a 0.030-inch outer diameter enclosed in a 3/16-inch tube flattened to a minimum inside dimension of 0.030 inch or an outside dimension of 0.075 inch. The 0.030-inch tubes were located as described and then silver-soldered in place. Each of the measuring stations was separated from the others by silver-solder partitions inside the tube.

The total-temperature rake (fig. 3(b)) consisted of three thermocouples located in a 3/16-inch tube flattened to an outside dimension of 0.075 inch. Fiber partitions were used to separate adjacent measuring stations so as to prevent air leakage between stations. The outer dimensions of the temperature and pressure rakes were the same.

All temperatures were measured with calibrated iron-constantan thermocouples. All interstage total-pressure rakes were connected to read the difference in pressure across a stage. These differences were measured on a common-well manometer with tetrabromoethane as the measuring fluid.

METHODS

The radial distribution of velocity after each blade row was determined by the method of reference 4, which requires a knowledge

of the total pressures, temperatures, and relative flow-angle distributions at a given mass flow. The method is based on a simultaneous solution of the energy and continuity equations. In determining the velocity distribution after a stator-blade row, the method was developed with the assumption that the condition of simple radial equilibrium was satisfied and that the entropy was constant along the radius after a stator-blade row. The assumption of constant entropy restricts the analysis to the determination of velocities in regions outside the boundary layers. The procedure used in calculating the velocity distribution after a rotor is general, however, in that the radial displacement of the flow in passing through the rotor was considered and the assumption of constant entropy was unnecessary.

It was found that the method was unsatisfactory for determining accurate values of velocity in several of the blade rows at certain operating points. In some instances, it was necessary to revise the method slightly so as to obtain velocity trends. The fact that the method was inapplicable in some blade rows indicates that the flow in these blade rows did not satisfy the ideal assumptions made in the method. The flow conditions that make the method invalid will be discussed in detail in the section "Results and Discussion."

Although the measurements of the total pressures and temperatures were made within the stator rows, it was assumed that the distributions of these quantities at the inlet and outlet of the blade rows were the same as those indicated by the instruments; that is, viscosity and heat-transfer losses and radial shifts in the energy distribution were neglected within the stator rows. The effects of the hub- and tip-wall boundary layers that would result from wall friction were completely neglected in the calculations. The effects of blade wakes resulting from friction along the blade surfaces were also neglected in determining the velocities out of the stationary-blade rows. It is believed, however, that the effects of the wakes on the integrated energy level and therefore on the effective flow area after the rotor blades were partly indicated on the instrument readings in the stator rows so that some mean velocity distribution was calculated after the rotor rows. The observed values of total pressure and temperature at the measuring stations in each blade row were extrapolated to the hub and tip sections to provide data at these sections.

The flow angles at the exit from the inlet guide vanes were determined from the three-dimensional cascade investigation of reference 5, assuming that the effect of the rotor on these angles would be small. At the peak-efficiency point, the relative flow angles out of each blade row, except the inlet guide vanes, were determined by

the rule of Carter and Hughes (reference 6) using the known blade geometry. The use of the Carter and Hughes rule assumes that each blade row is operating near the design angle of incidence. In order to determine the flow angles for the maximum weight flow and surge points, it was assumed that the variation of turning angle with angle of incidence was a straight line of slope 0.9 passing through the point determined for the peak-efficiency operating condition; that is, a 1° change in the angle of incidence caused a 0.9° change in turning angle. In the actual case, the slope of the line variation of incidence and turning angle has been found to vary with solidity, stagger, and blade shape. The assumption of the straight-line variation implies that the high and low incidence values, at which a large drop in turning angle (stall) occurs, are never encountered for the range of conditions investigated here. An indication of the effect of errors in flow angle is shown in reference 4. An error of 2° in the angle out of the fourth-rotor discharge resulted in a maximum error of 1.5 percent in the axial velocity.

Because the derivation of the basic calculation method for the stator rows was completely independent of conditions upstream of these blade rows and because of the method of determining flow angle, the calculation of the velocities out of the stator was only slightly affected by conditions upstream of the stator rows. Any errors that arose in the calculation of the rotor-exit velocities would therefore not be accumulative.

RESULTS AND DISCUSSION

Over-All Performance of Compressor at Survey Points

The over-all performance of the compressor operating at the design speed with an inlet-air pressure of 12 inches of mercury absolute and ambient inlet-air temperature with the interstage instrumentation installed is compared with the performance with no instrumentation (determined from reference 2) in figure 4. Before the stage-performance investigation was run, however, a failure of one of the setup parts caused the rotor-blade tips to rub slightly and made it necessary to replace the outlet guide vanes. The effect of the failure as indicated in reference 2 was small. The differences in performance shown in figure 4 are therefore caused principally by the effect of interstage instrumentation and also by possible effects of heat transfer. During the investigation of reference 2, the compressor was insulated to minimize external heat transfer, whereas it was not insulated in the present investigation. The indicated performance of the compressor with the instrumentation

installed appears to have been increased slightly as evidenced by the increase in maximum efficiency from 0.79 to 0.80 (fig. 4(a)) and the increase in total-pressure ratio from 3.30 to 3.46 (fig. 4(b)). The effect on efficiency appears to be in the direction expected of a heat-transfer effect. The effect on pressure ratio, however, indicates that the effect of the instruments is to improve the stage-matching characteristics of the compressor, giving a higher over-all pressure ratio than was obtained without interstage instruments. The effect of the instrumentation on the maximum equivalent weight flow is negligible, however.

Measured Interstage Data and Stage Pressure Ratios

The measured interstage total pressures and temperatures for the peak-efficiency point are presented in figure 5 as ratios of the measured interstage values to the compressor-inlet pressure to indicate the trends and the extent of the observed data. The extrapolations of the pressure and temperature data to the hub and tip sections are also shown to indicate the values used at these locations in the calculation of the interstage velocities. Throughout the compressor, the total pressure is lower near the hub than near the tip (fig. 5(a)). The maximum gradient of total pressure occurs in the middle stages. The total pressure in the tenth stator is practically constant with a maximum variation of less than 2 percent. Similar trends of measured total pressures were followed at the maximum weight-flow and surge operating points in all stages except the tenth stator. In this blade row, the total pressure decreases from hub to tip for the maximum weight-flow point and increases from hub to tip at the surge point.

The trends of the measured total-temperature distributions generally follow those of the total pressures in the first five stages of the compressor (fig. 5(b)). On the basis of the data obtained, however, it appears that a minimum temperature occurs near the mid-span of the passage annulus in the last five stages. In every case, however, the maximum temperature occurs near the tip. The temperature trends indicated in figure 5(b) are similar in shape to those at the maximum weight-flow and surge points.

Using the total pressures measured in each stator row, the stage total-pressure ratios were calculated and are plotted in figure 6 at the three measuring stations as functions of the compressor-inlet equivalent weight flow. The pressure ratios of all except the first stage were determined by dividing the measured pressure at any

station by the measured pressure at the corresponding measuring station in the previous stage. The first-stage pressure ratio was obtained by dividing the pressure measured in the first stator by the pressure in the depression tank. In the first stage, the arithmetically averaged pressure ratio at the surge point was 1.10 and in the second stage, approximately 1.13. In all other stages, the average stage pressure ratio was approximately 1.15.

From figure 6, it can be seen that a large radial gradient in total-pressure ratio from a value of less than 1.00 at the hub to 1.20 at the outer measuring station at the surge point is set up in the first stage. Inasmuch as the first rotor hub was designed to do no work and the first-stage pressure ratio includes inlet losses, the pressure ratio of less than 1.00 near the hub indicates inlet losses or a turbine-like effect. A turbine-like effect was indicated by the slightly negative incidence angle at this blade section.

The radial variation of stage pressure ratio set up in the first stage is seen to be reversed in the third stage so that, except for the surge point, a higher stage pressure ratio was obtained at the hub section than at the tip. In the fourth stage, the pressure ratio was practically constant at all radial positions. From the fifth stage on, a greater stage pressure ratio occurred at the hub than at the tip, so that the large gradient of total pressure set up in the first stage was gradually reduced to almost a constant value of total pressure at all radii in the last stage. The reversal in the radial gradient of total-pressure ratio was accomplished primarily by a reversal in the camber distribution (fig. 1).

The variation of stage pressure ratio with weight flow is slight in the initial stages but increases after the fifth stage such that the pressure ratio is noticeably increased as the weight flow is reduced from the maximum flow to the peak-efficiency point. At flows below that at the peak-efficiency point, the pressure ratio in each of the later stages appears to be leveling off. Thus it appears that the drop in stage pressure ratio between the peak-efficiency and surge points in the early stages cannot be entirely recovered by the later stages. It should be remembered that in the curves of figure 6, the compressor-inlet-air conditions were used to determine the equivalent weight flow. If the conditions at the inlet to each blade row had been used as the weight-flow parameter, the indicated range of weight flow at the high-pressure regions would have been extended as is the range of angle of attack in these blade rows. The trends would, however, be the same as those shown in figure 6.

[redacted]

Velocity-Diagram Calculations

Comparison of measured and calculated wall static pressures. - An indication of the accuracy of the velocity calculations was made by comparing the calculated static pressure at the tip section of each blade row with the measured value at this section at the peak-efficiency operating condition in figure 7. The static pressures are presented as the ratio of the static pressure at each station to the compressor-inlet total pressure. The radial distribution of static pressure was calculated from the measured radial distributions of total pressure and total temperature and the calculated distribution of velocity after each blade row. Circumferential variations in measured static pressure between blades were assumed to be small. The variation from one measuring station to the next was also neglected because the variation of total pressure at the three circumferential measuring stations was small.

At the rotor discharge, the calculated static pressures checked the measured pressures within 2 to 4 percent in the first five blade rows and within 2 percent in the last four rows (fig. 7(a)). These errors are equivalent to 1 to 14 percent of the velocity head in the first five rotors and 1 to 6 percent of the velocity head in the last four rotors. A leak in the manometer tube made it impossible to measure the wall static pressure after the sixth rotor. In the stators, the difference between the measured and calculated wall static pressures was 1 to 3 percent in the first eight rows, with a difference of 5 percent in the last two rows. As percentages of the velocity head, these differences in static pressures were equivalent to a variation of 5 to 15 percent in the first eight stators with progressively increasing differences of 25, 45, and 74 percent in the ninth stator, tenth stator, and outlet guide vanes, respectively.

Although the agreement of the static pressures in the third, fourth, and fifth stators is fairly good at the peak-efficiency point, it was found that at the surge point the continuity equation could not be satisfied in these blade rows. The revised calculation procedure used at the surge point resulted in a calculated static pressure that was slightly lower than the measured value. The progressively increasing errors in the last three stationary blade rows of the compressor indicate the accumulation of wakes and boundary layers in the latter stages of the compressor, thus making the calculation method inapplicable in these stator rows. As indicated earlier, the effects of wakes after the rotor rows are distributed over the full annulus area by the measurements in the stator rows.

General trends of velocity diagrams. - The calculated values of the velocities and flow angles along three streamlines through the compressor are presented in table I for the three operating points investigated. The streamlines are determined as the lines passing through the centers of three equal increments of mass flow. The streamline near the hub is designated a; near the mean section, b; and near the tip, c. The radial positions (table I) of the streamlines before and after each rotor-blade row indicate that the flow is displaced radially inward in the rotor and outward in the stator with the largest displacements occurring along streamline a. Because the magnitudes of these displacements depend to a large extent on the boundary-layer configurations along the annulus walls, which were not determined in the present investigation, the magnitudes of the displacements cannot be accurately evaluated. The calculations indicate, however, that there is a definite oscillatory motion throughout the compressor, as denoted in reference 8.

Because the general trends of the velocity distributions are similar at the three operating points, figure 8 presents the calculated velocity diagrams along the three streamlines through the compressor at the peak-efficiency point. A sample vector diagram is presented in figure 9 to clarify the locations of the velocities and the nomenclature used.

With the exception of the tenth stage the radial distribution of the exit flow angle of each blade row is such that the relative tangential velocity entering the rotor is approximately equal to the tangential velocity entering the stator; the relative tangential velocity leaving the rotor and the tangential velocity leaving the stator are also approximately equal at all radii. The radial distribution of tangential velocity throughout the compressor therefore approaches that required of a symmetrical velocity diagram. When the conditions of a symmetrical velocity diagram at all radii are imposed on the tangential velocity, a mean velocity distribution similar to a wheel-type flow design results. In all rotors except the ninth, the blade speed and the radial distribution of blade exit angle combine to cause the absolute tangential velocity to increase with radius. In the ninth rotor, there is a minimum value of absolute tangential velocity at the mean section; however, the over-all variation from hub to tip is only 6 percent.

The calculations of axial velocity after the stators indicate a radial gradient in axial velocity, increasing from hub to tip, after all stator rows from the first to the seventh stages. The radial variations of axial velocity leaving the eighth and ninth stators are small. After the tenth stator, the axial velocity is practically constant.

[redacted]

Velocity diagrams in first and second stages. - The rotor blades used in the first two stages were identical, as indicated in figure 1, and differed appreciably from all other rotor blades. Therefore, as was shown in figure 6, the radial gradient of work (increasing from hub to tip) in these first two stages differed from that in all other stages. Although the blade profiles were identical, differences in the distributions of the angle of incidence cause the radial gradient of work in the second rotor to be slight when compared with the gradient in the first rotor.

As indicated in figure 8, the radial distribution of turning angle in the inlet guide vanes is such as to give a linear distribution of flow angle into the first rotor with the flow angle increasing from hub to tip. The angle of incidence at the peak-efficiency point (determined from the flow angle and the blade inlet angle presented in fig. 2) at the first rotor varies from a small negative value near the hub to approximately 10° near the tip. The camber angle varied approximately 8° across the annulus in the first rotor (fig. 1) with the hub section having a symmetrical airfoil section; thus the large gradient of work (increasing from hub to tip) in the first rotor row was accomplished by the combination of the variation of inlet flow angle or angle of incidence and the variation of camber angle. The slightly negative incidence angle at streamline a in the first rotor indicates a slight turbine-like effect at this section, as is also indicated in figure 6.

At the peak-efficiency point, the radial distribution of relative velocity leaving the first rotor is such that the following stator row is operating at very small angles of incidence at all radii. The change in the angular momentum in the first stator increases gradually from hub to tip in accordance with the distribution of camber presented in figure 1. It is the combination of this camber distribution and the axial-velocity distribution set up by the first rotor that causes the radial distribution of angle of incidence into the second rotor to be approximately uniform along the radius. The difference in the work distribution between the first and second stages is attributed entirely to the change in the radial distribution of angle of incidence.

Velocity diagrams in third, fourth, and fifth stages. - The third, fourth, and fifth stages are discussed as a group because the rotor-blade sections are identical and the stators are similar, and because it was in the stator rows of these stages that the calculation method could not be satisfactorily applied to determine the axial-velocity distributions at the surge point. The indications are that thick boundary layers accumulate in the hub region of these stages causing the flow to separate from the blades and recirculate back into the blade row.

The velocities in the stator rows of these stages have almost identical distributions, as shown in figures 8(c) to (e), with low values of velocity at a and high values at c. In order to give a more complete description of the unusual velocity trends in the third, fourth, and fifth stators, the radial distribution of axial velocity after the fourth stator is presented in figure 10 as the ratio of axial velocity to rotor-blade tip speed for the three operating points investigated. Also shown is the radial distribution of axial velocity at the surge point that would occur if the annular passage were reduced to an "equivalent" annulus that passed the measured weight flow when the axial velocity at the equivalent hub was zero. The difference in radius between the geometrical hub and the equivalent hub was 0.425 inch corresponding to approximately 10 percent of the blade height. Thus, in effect, an indication of the extent of the boundary layer near the hub was obtained. Because of the thin trailing edges (0.010 in.) of the airfoil sections used, it is believed that the effect of blade wakes on effective flow area was small except in the regions where boundary-layer separation occurred in the blade surfaces and interacted with the annulus wall boundary layer. If boundary layers were completely neglected, it would be necessary to assume imaginary values of velocity near the stator hub in order that the measured weight flow and the weight flow determined by integrating the velocity curve be equal at the surge point. For this reason, the calculation procedure presented in reference 4 was revised for application to the third, fourth, and fifth stators at the surge point. The revision consisted in neglecting the continuity requirement so that the velocities after the third, fourth, and fifth stators were determined by assuming that the axial velocity at the hub was zero. The velocity distributions shown in table I at the surge point for the third, fourth, and fifth stators therefore result in weight flows that differ by 8 percent, 14 percent, and 7 percent, respectively, from the measured weight flows. The determination of the equivalent hub dimension assumes that no flow passed through the annular region between the annular hub and the equivalent hub. If a recirculating flow existed near the hub such that the flow was toward the compressor inlet at the hub section, the point at which the axial velocity is zero would actually be closer to the hub than the equivalent hub radius indicated in figure 10. Whereas the axial-velocity distribution determined from the revised calculation method at the surge point gave a calculated wall static pressure that was slightly lower than the measured pressure, the velocity distribution for the equivalent annulus gave a calculated pressure slightly higher than the measured value, indicating that the velocities were low. Therefore, as was expected, the effects of boundary layers have not been completely evaluated by the equivalent hub calculation.

[redacted]

A comparison of the curves of figure 10 indicates that a decrease in weight flow from maximum to surge results in a large decrease in the axial velocity in the inner portion of the annular passage and a slight increase in axial velocity near the tip. On the basis of the available data, it appears that as the weight flow is decreased, the boundary layer builds up until, at surge, the boundary layer separates and a recirculating flow occurs in the hub region. In order to determine the effect on the calculated velocities of an error in assumed flow angle, which would result if separation occurred, the turning angle at the hub of the fourth stator was decreased by 5° at the surge point. Because the effect of this change on the axial-velocity distribution was negligible, the velocity distribution was affected by the reduction in the effective flow area resulting from the increased boundary layer and blade wakes near the hub and not by the changes in the flow angles that might result if separation occurred in the stator. Because the unusual trends existed in the three stages simultaneously, the high camber angles (fig. 1) at the hub section in these rotors and stators required to compensate for the low turning at the hub sections of the first two rotors may have been the principle cause of the difficulty. Thus it appears that the large gradient of work set up in the first rotor cannot be reversed as rapidly as it was in the present case.

Velocity diagrams in sixth, seventh, and eighth stages. - Although the general trends of velocity in the sixth, seventh, and eighth stages are similar to those in the three preceding stages, it is of interest to note from figure 8 that the large radial gradients of velocity set up in the third, fourth, and fifth stators are gradually reduced in these stages. It appears that the reduced camber angles at the hub of these stages make it possible to operate efficiently even at the somewhat high values of incidence that result from the low axial velocities entering the hub section of the sixth rotor. The measured data therefore indicate that even if certain blade rows are operating at unfavorable conditions, succeeding stages can be designed so as to cause the flow to smooth out and return to a satisfactory distribution.

Velocity diagrams in ninth and tenth stages. - The progressively increasing differences between the measured and calculated wall static pressures (fig. 7(b)) in the last three stationary-blade rows of the compressor, indicate the accumulation of blade wakes and wall boundary layers in these last three blade rows. Part of the boundary-layer accumulation may result from separation and backflow at the hub sections of the ninth and tenth stages similar to that which occurred in the third, fourth, and fifth stages. The extremely large errors in wall static pressures and the nearly constant total pressure after the tenth stator (fig. 5(a)) indicate large reductions in effective

flow areas resulting primarily from wakes. Calculations based on the differences between the measured and calculated static pressures have indicated that wakes, boundary layers, or recirculating flows caused a reduction in effective flow area of 15 percent of the geometrical annulus area after the tenth stator and 25 percent after the outlet guide vanes. The fact that the wall static pressures after the rotors in these later stages do not indicate large errors (fig. 7(a)) serves to emphasize the importance of the blade wakes in reducing the effective flow area. The wakes after the rotors are indirectly accounted for by the measured total pressures but the wakes after the stators are completely neglected. The calculations after the rotors therefore give some mean value of velocity distribution.

With the exception of the tenth stator, the last two stages are operating at moderate angles of incidence at all radii at the peak-efficiency point. The angle of incidence at the hub of the tenth stator, however, is approximately -14°. The combination of this large negative incidence and the high stagger of this blade row makes it appear likely that this section is either stalling or is approaching a stall condition.

The Reynolds numbers determined from the calculated velocity distributions indicate values that vary from 100,000 to 180,000 with the lowest Reynolds numbers occurring in the initial stages. The data presented in reference 9 indicate that the initial stages of the present compressor may be operating in the critical Reynolds number range, in which a slight change in Reynolds number causes a large change in performance. It should be noted that the effective Reynolds numbers in the later stages of the compressor are even higher than those calculated because of the turbulence that develops through the compressor.

SUMMARY OF RESULTS

The results of the investigation of the stage performance of the X24C-2 ten-stage axial-flow compressor at the design speed are summarized as follows:

1. The average stage total-pressure ratio at the surge operating condition in the first stage was approximately 1.10 and in the second stage was approximately 1.13. In all the remaining stages, the average total-pressure ratio at the surge point was approximately constant at a value of 1.15.

[redacted]

2. The large radial gradient of stage pressure ratio, increasing from less than 1.00 at the hub to 1.20 near the tip at the surge point, set up in the first stage was reduced in the second stage. In all stages after the second stage, with the exception of the fourth stage, the radial gradient of stage pressure ratio set up in the first stage was reversed by a reversal in the radial distribution of camber angle so that the large gradient of total pressure set up in the first stage was gradually reduced to almost a constant total pressure at the compressor outlet. The stage pressure ratio in the fourth stage was practically constant at all radii.

3. The high turnings required at the hub of the third, fourth, and fifth stages in order to compensate for the low turnings in the first two stages appeared to cause the gradual build-up in boundary layer as the weight flow was reduced until at the surge point, the boundary layer separated and a recirculating flow occurred in these highly loaded blade sections.

4. The data indicated the accumulation of blade wakes and boundary layers in the last three stationary blade rows of the compressor causing the effective flow area after the outlet guide vanes to be reduced by approximately 25 percent of the geometrical annulus area at the peak-efficiency point. The effect of the blade wakes appears to be of primary importance.

5. The radial distribution of tangential velocity in each stage was such that the conditions of a symmetrical velocity diagram were being approached at almost all sections.

1319

Lewis Flight Propulsion Laboratory,
National Advisory Committee for Aeronautics,
Cleveland, Ohio, March 27, 1950.

Harold B. Finger

Harold B. Finger,
Aeronautical Research
Scientist.

Leo Cohen

Leo Cohen,
Aeronautical Research
Scientist.

Warner L. Stewart

Warner L. Stewart,
Scientific Aid.

Approved: Robert O. Bullock

Robert O. Bullock,
Aeronautical Research
Scientist.

Oscar W. Schey

Oscar W. Schey,
Aeronautical Research
Scientist.

jml

[redacted]

APPENDIX - SYMBOLS

The following symbols are used in the figures:

i	incidence angle, angle between blade inlet and air direction, deg
P	total pressure, lb/sq ft absolute
p	static pressure, lb/sq ft absolute
r	radius, ft
T	total temperature, $^{\circ}R$
U	blade element speed, ft/sec
V	absolute air velocity, ft/sec
V'	velocity relative to rotor row, ft/sec
W	weight flow, lb/sec
α	camber angle, deg
β	angle between absolute velocity and axial direction, deg
β'	angle between relative air velocity and axial direction, deg
δ	ratio of inlet-air total pressure to NACA standard sea-level pressure
η_T	adiabatic temperature-rise efficiency
ζ	blade inlet angle, angle between camber line at leading edge of airfoil and axial direction, deg
θ	ratio of inlet-air total temperature to NACA standard sea-level temperature

Subscripts:

i	compressor inlet
o	compressor outlet
t	tip

[redacted]

z axial

θ tangential

1 rotor inlet

2 stator inlet or rotor outlet

3 stator outlet (equivalent to following rotor inlet)

REFERENCES

1. Schum, Harold J., and Buckner, Howard A., Jr.: Investigation of 10-Stage Axial-Flow X24C-2 Compressor. I - Performance at Inlet Pressure of 21 Inches Mercury Absolute and Inlet Temperature of 538° R. NACA RM E7G11, Bur. Aero., 1947.

2. Finger, Harold B., Schum, Harold J., and Buckner, Howard A., Jr.: Investigation of X24C-2 10-Stage Axial-Flow Compressor. II - Effect of Inlet-Air Pressure and Temperature on Performance. NACA RM E7H22, Bur. Aero., 1947.

3. Buckner, Howard A., Jr., and Downing, Richard M.: Investigation of X24C-2 10-Stage Axial-Flow Compressor. III - Surge Characteristics. NACA RM SE8H06, Bur. Aero., 1948.

4. Finger, Harold B.: Method of Experimentally Determining Radial Distributions of Velocity through Axial-Flow Compressor. NACA TN 2059, 1950.

5. Finger, Harold B., Schum, Harold J., and Buckner, Howard A., Jr.: Experimental and Theoretical Distribution of Flow Produced by Inlet Guide Vanes of an Axial-Flow Compressor. NACA TN 1954, 1949. (Formerly RM E8J27.)

6. Carter, A. D. S., and Hughes, Hazel P.: A Theoretical Investigation into the Effect of Profile Shape on the Performance of Airfoils in Cascade. Power Jets Rep. No. R1192, Res. and Development, Power Jets, Ltd., March 1946.

7. NACA Subcommittee on Compressors: Standard Procedures for Rating and Testing Multistage Axial-Flow Compressors. NACA TN 1138, 1946.

[redacted]

8. Wu, Chung-Hua, and Wolfenstein, Lincoln: Application of Radial-Equilibrium Condition to Axial-Flow Compressor and Turbine Design. NACA Rep. 955, 1950. (Formerly NACA TN 1795.)

9. Eckert, B.: The Influence of Physical Dimensions (Such as Hub: Tip, Ratio, Clearance, Blade Shape) and Flow Conditions (Such as Reynolds Number and Mach Number) on Compressor Characteristics. Part A - Summary of the Results of Research on Axial Flow Compressors at the Stuttgart Research Institute for Automobiles and Engines. W.A.C. Eng. Trans. No. 22, Wright Aero. Corp. (Vol. 3 of series of articles on compressor and fan design, written by German engineers, coordinated by Code 338, BuShips, Navy Dept. (Washington, D.C.), May 1946.

[redacted]

INDEX OF FIGURES

[redacted]

Figure 9. - Velocity-diagram notation.

Figure 10. - Radial distribution of axial velocity after fourth stator for various weight flows showing effect of boundary layer at hub at surge.

DISTRIBUTION ON STREAMLINES a, b, AND c[1]

Rotor number	$\frac{r_1}{r_t}$	$\frac{r_2}{r_t}$	$\frac{V_1}{U_t}$	$\frac{V_2}{U_t}$	$\frac{V'_1}{U_t}$	$\frac{V'_2}{U_t}$	$\frac{V_{z,1}}{U_t}$	$\frac{V_{z,2}}{U_t}$	$\frac{V_{\theta,1}}{U_t}$	$\frac{V_{\theta,2}}{U_t}$	$\frac{V'_{\theta,1}}{U_t}$	$\frac{V'_{\theta,2}}{U_t}$	β_1 (deg)	β_2 (deg)	β'_1 (deg)	β'_2 (deg)
Peak-efficiency point - Concluded																
6a	0.72	0.71	0.44	0.63	0.63	0.46	0.38	0.40	0.22	0.48	0.50	0.23	30	50	53	29
b	.86	.84	.59	.68	.69	.55	.47	.45	.35	.52	.51	.32	37	49	47	36
c	.96	.95	.68	.75	.76	.60	.53	.47	.42	.58	.56	.37	38	51	45	38
7a	.74	.72	.46	.65	.64	.53	.39	.46	.23	.46	.50	.26	31	45	53	29
b	.86	.84	.57	.67	.69	.52	.45	.41	.35	.53	.51	.31	37	52	49	37
c	.96	.95	.64	.73	.74	.58	.49	.45	.41	.58	.55	.37	40	52	48	40
8a	.75	.75	.48	.66	.64	.52	.41	.44	.25	.48	.50	.27	32	48	51	31
b	.87	.86	.56	.68	.68	.53	.44	.42	.35	.53	.52	.33	39	51	49	38
c	.96	.96	.62	.72	.72	.58	.47	.44	.41	.57	.54	.38	42	53	49	41
9a	.77	.78	.48	.68	.69	.48	.43	.42	.22	.54	.55	.24	27	52	52	30
b	.87	.88	.55	.69	.71	.59	.45	.46	.32	.51	.55	.37	35	48	51	39
c	.96	.96	.59	.71	.70	.63	.43	.47	.40	.54	.56	.42	43	49	52	42
10a	.79	.77	.50	.74	.71	.65	.44	.57	.23	.47	.56	.30	27	39	52	28
b	.88	.86	.53	.68	.72	.46	.44	.36	.30	.57	.57	.29	35	58	53	39
c	.96	.96	.56	.71	.72	.50	.42	.36	.37	.61	.59	.35	42	60	55	44
20.G.V.a	.78	.79	.49	.36			.39	.36	.30	.03			38	5		
b	.88	.88	.49	.38			.39	.38	.30	.03			38	5		
c	.96	.96	.49	.40			.39	.40	.30	.04			38	5		
Surge point																
1a	0.60	0.63	0.66	0.63	0.69	0.59	0.61	0.52	0.26	0.35	0.34	0.27	23	34	30	28
b	.78	.81	.63	.73	.74	.66	.55	.56	.29	.46	.49	.34	28	40	41	31
c	.93	.94	.61	.80	.83	.71	.53	.59	.29	.54	.64	.40	29	43	50	34
2a	.64	.63	.53	.58	.60	.53	.46	.46	.26	.36	.37	.27	30	38	39	31
b	.82	.81	.66	.69	.71	.63	.55	.52	.36	.46	.45	.35	34	41	40	34
c	.95	.94	.74	.76	.79	.65	.60	.52	.43	.55	.51	.39	36	47	40	37
3a	.66	.61	.44	.65	.64	.54	.41	.50	.17	.41	.49	.20	23	40	50	22
b	.83	.79	.61	.66	.72	.51	.52	.43	.33	.51	.50	.28	32	50	44	34
c	.95	.94	.71	.75	.78	.54	.57	.43	.42	.61	.53	.33	37	55	43	37
4a	.68	.65	.48	.60	.63	.33	.43	.30	.22	.52	.47	.13	27	60	47	23
b	.84	.83	.64	.69	.72	.50	.53	.41	.35	.55	.49	.28	34	53	43	34
c	.95	.95	.71	.76	.80	.67	.58	.53	.40	.54	.55	.41	35	46	43	38
5a	.71	.67	.50	.63	.63	.38	.44	.35	.24	.52	.46	.15	29	56	47	23
b	.85	.83	.66	.69	.71	.53	.54	.44	.38	.53	.47	.30	35	50	41	34
c	.95	.95	.73	.74	.78	.54	.58	.42	.43	.61	.52	.34	37	56	42	39
6a	.74	.71	.47	.62	.63	.38	.41	.33	.24	.52	.50	.19	31	58	51	30
b	.86	.85	.62	.69	.70	.51	.50	.41	.37	.55	.49	.30	37	54	45	36
c	.96	.96	.69	.75	.76	.59	.54	.47	.43	.59	.53	.37	38	52	44	38
7a	.76	.73	.44	.63	.64	.40	.37	.34	.24	.53	.52	.20	33	57	55	31
b	.87	.85	.58	.68	.69	.54	.45	.43	.35	.53	.52	.32	38	51	49	37
c	.96	.95	.64	.74	.74	.53	.49	.41	.41	.61	.55	.34	40	56	48	40
8a	.76	.76	.41	.64	.64	.44	.34	.37	.22	.52	.54	.23	33	55	58	32
b	.87	.87	.54	.68	.68	.52	.42	.40	.33	.54	.54	.32	38	53	52	39
c	.96	.96	.60	.73	.71	.53	.44	.40	.40	.61	.56	.35	42	57	52	41
9a	.78	.77	.40	.68	.68	.42	.35	.36	.19	.57	.59	.20	29	57	59	29
b	.88	.87	.51	.68	.71	.50	.41	.39	.30	.56	.58	.31	36	55	54	39
c	.96	.96	.58	.71	.70	.57	.42	.42	.40	.58	.56	.38	43	54	53	42
10a	.79	.77	.40	.69	.70	.52	.36	.45	.19	.52	.60	.25	28	49	59	29
b	.89	.86	.50	.69	.71	.39	.40	.30	.29	.62	.59	.25	36	64	56	39
c	.96	.96	.54	.71	.72	.50	.40	.36	.37	.61	.60	.35	42	60	56	44
20.G.V.a	.79	.80	.39	.27			.31		.24	.03			38	5		
b	.89	.89	.43	.35			.34		.27	.03			38	5		
c	.96	.97	.46	.40			.37		.28	.04			38	5		

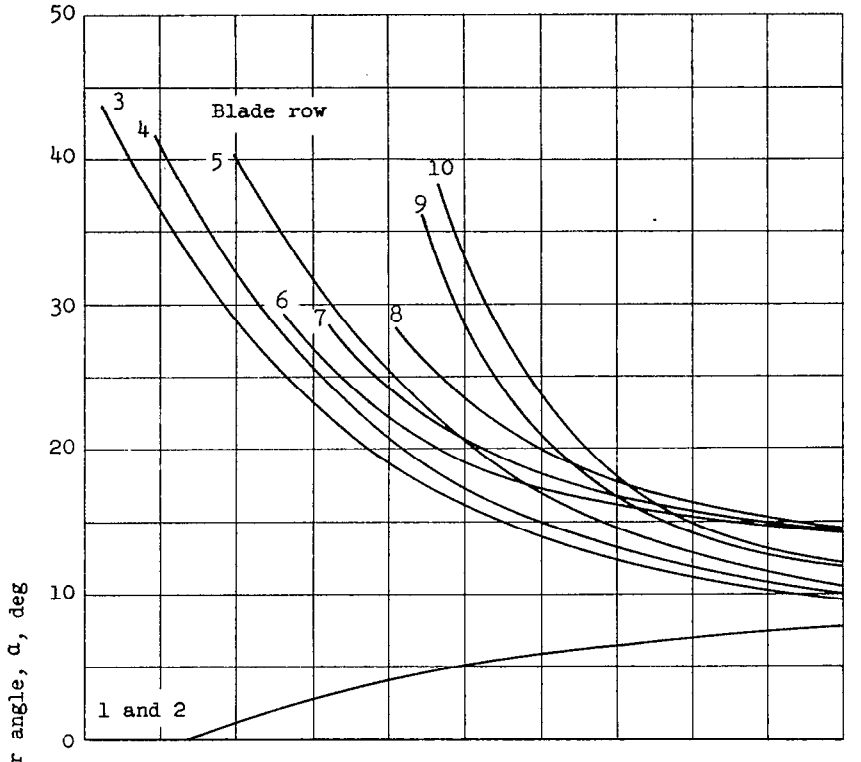

(a) Rotor blades.

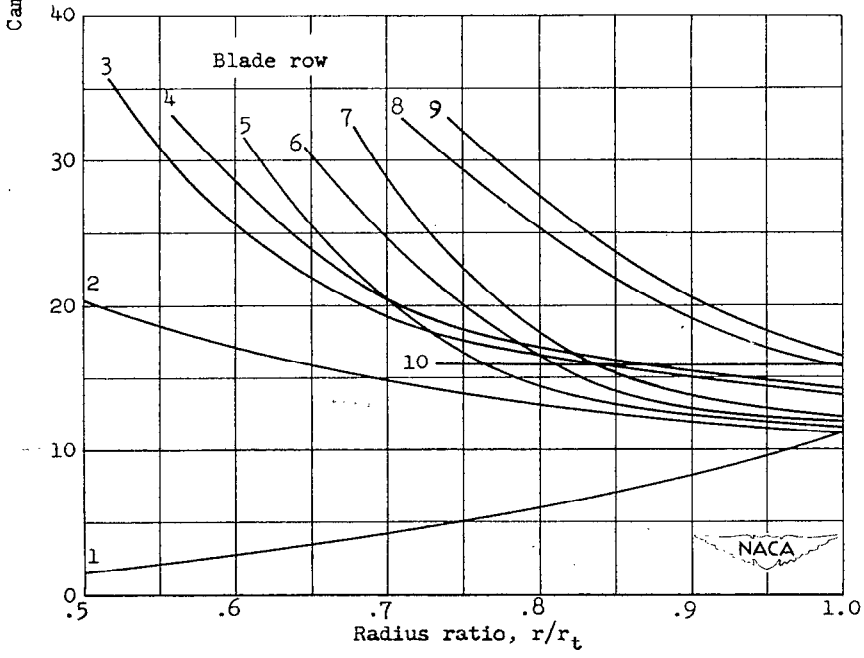

(b) Stator blades.

Figure 1. - Radial variation of camber angle for all blade rows.

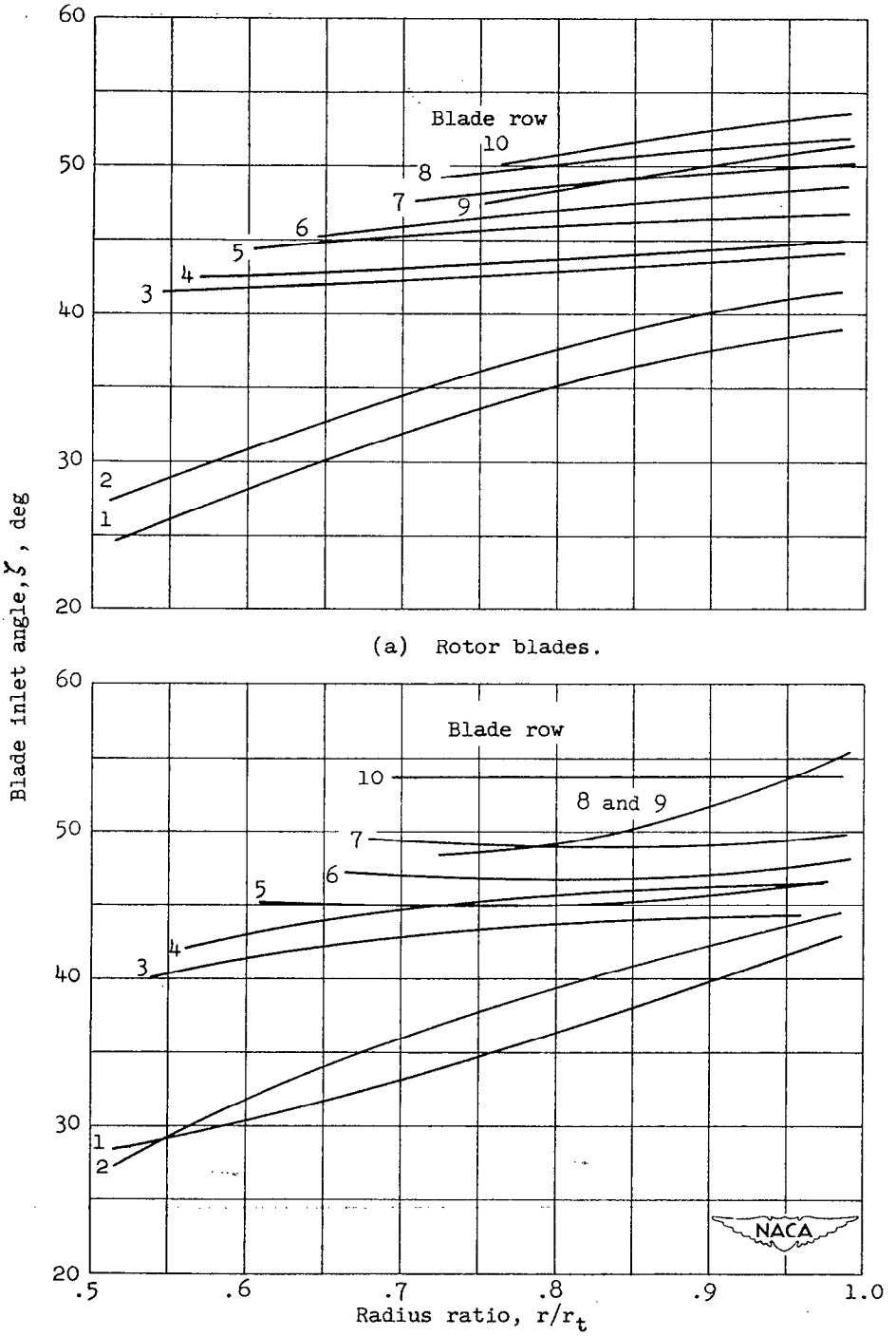

(a) Rotor blades.

(b) Stator blades.

Figure 2. - Radial variation of blade inlet angle for all blade rows.

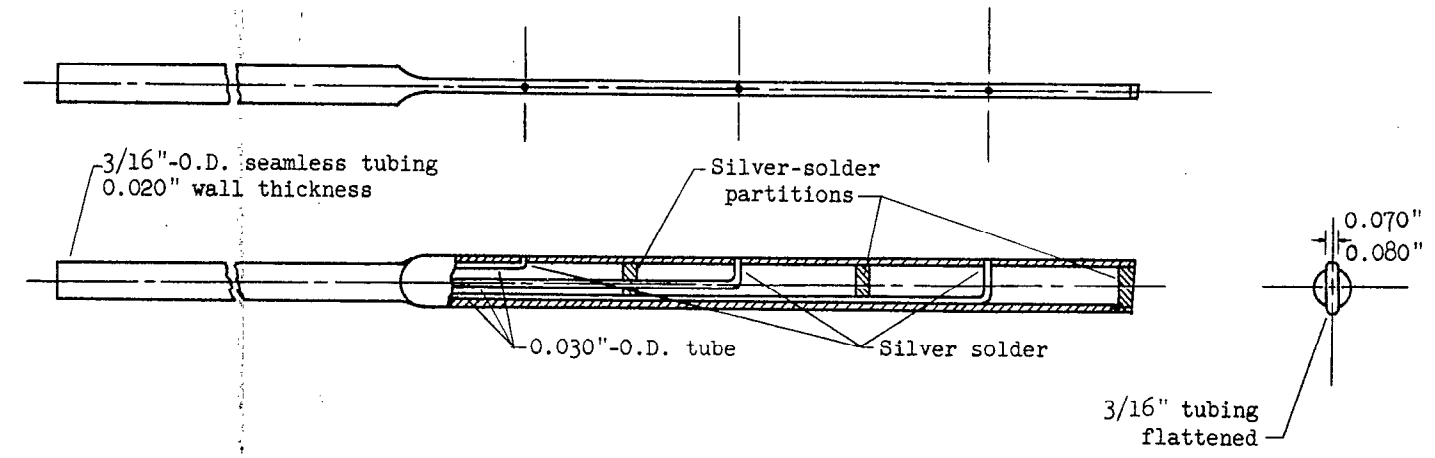

(a) Total-pressure rake.

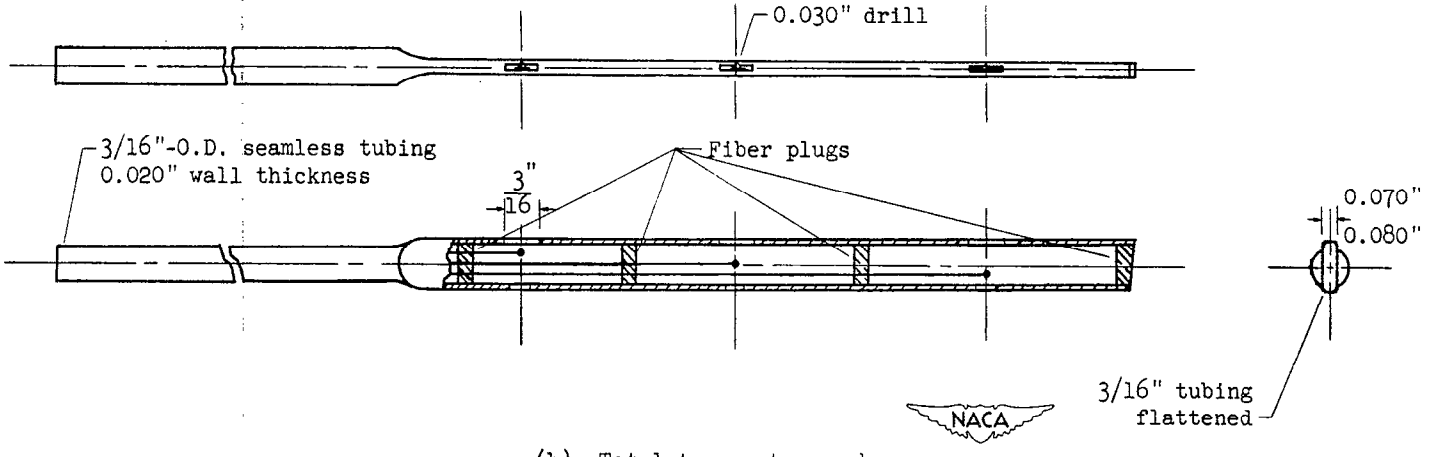

(b) Total-temperature rake.

Figure 3. - Interstage measuring probe.

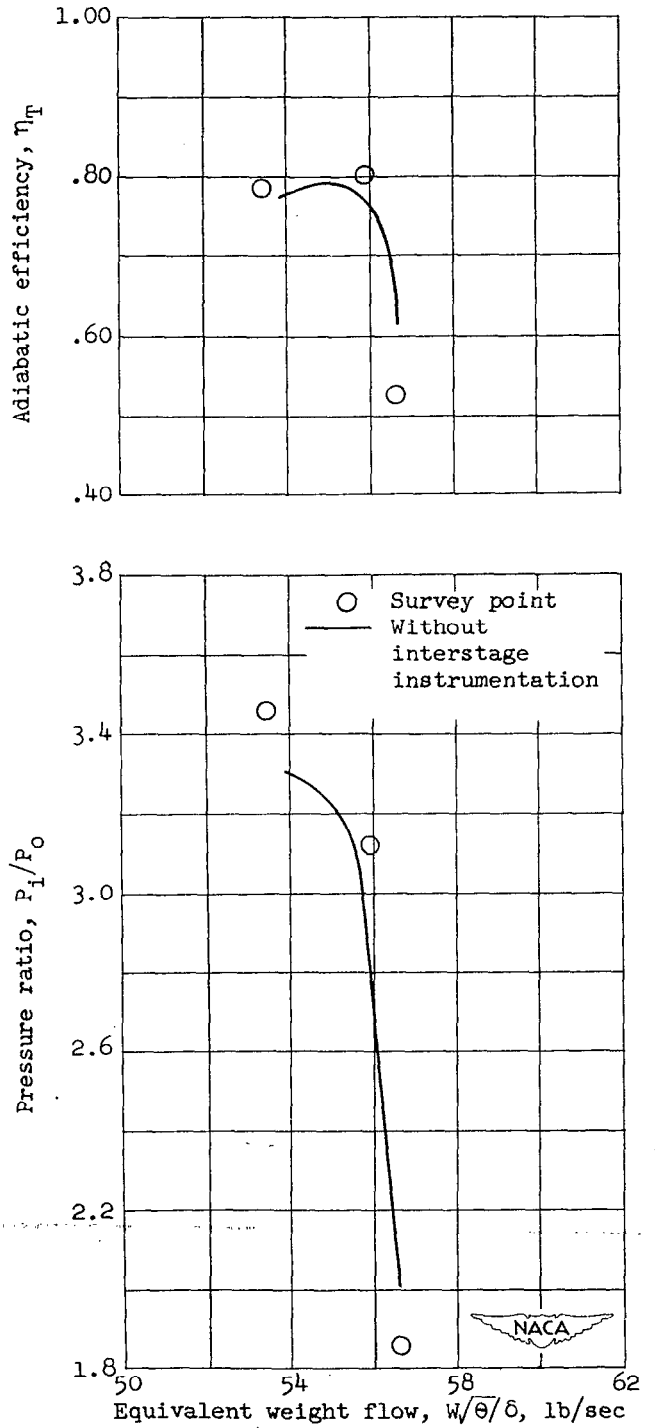

Figure 4. - Over-all performance of 10-stage compressor at three survey points showing effect of instrumentation.

[redacted]

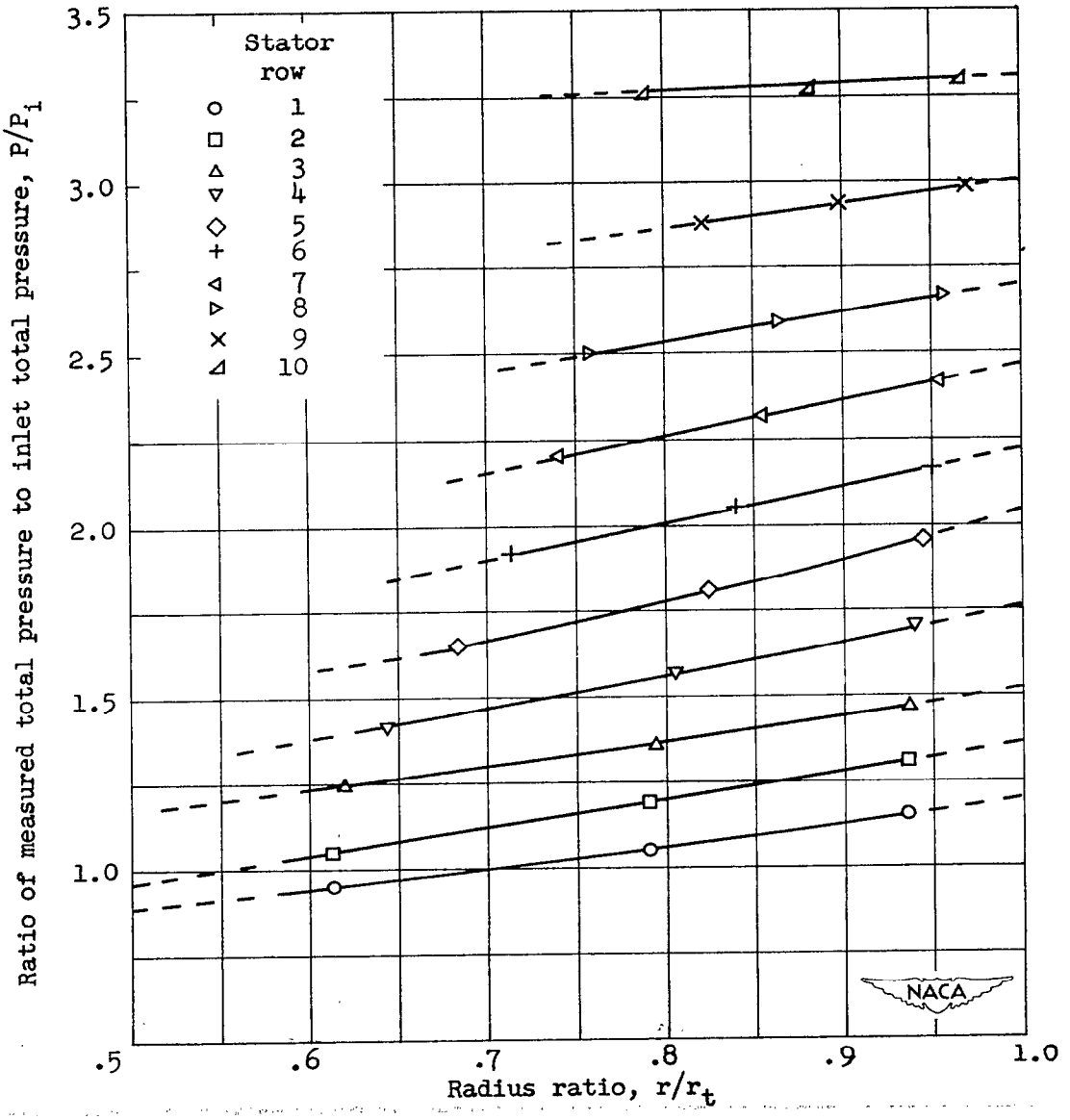

(a) Variation of measured total-pressure ratio with radius ratio.

Figure 5. - Performance data measured in each stator row at compressor peak-efficiency operating point.

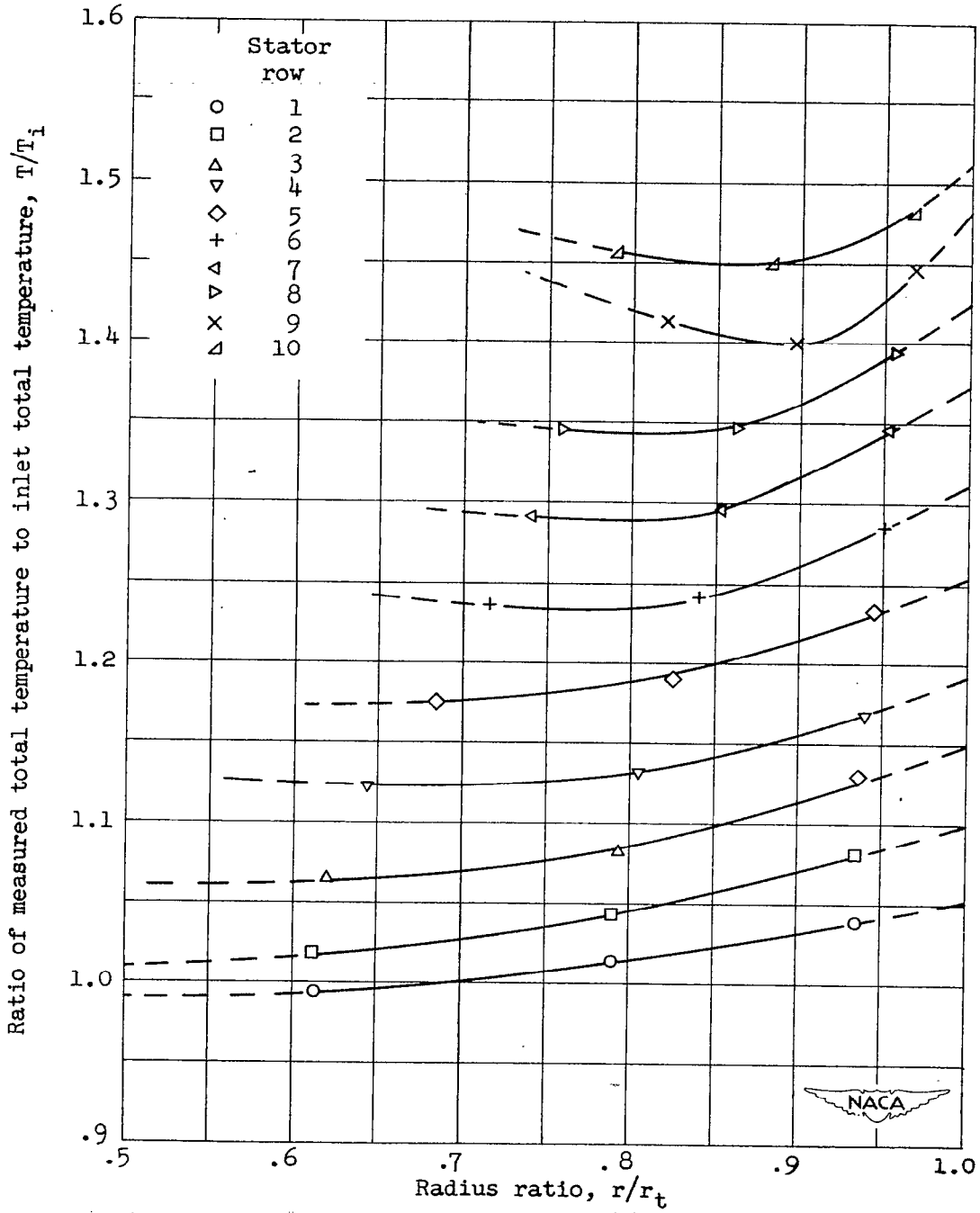

(b) Variation of measured total-temperature ratio with radius ratio.

Figure 5. - Concluded. Performance data measured in each stator row at compressor peak-efficiency operating point.

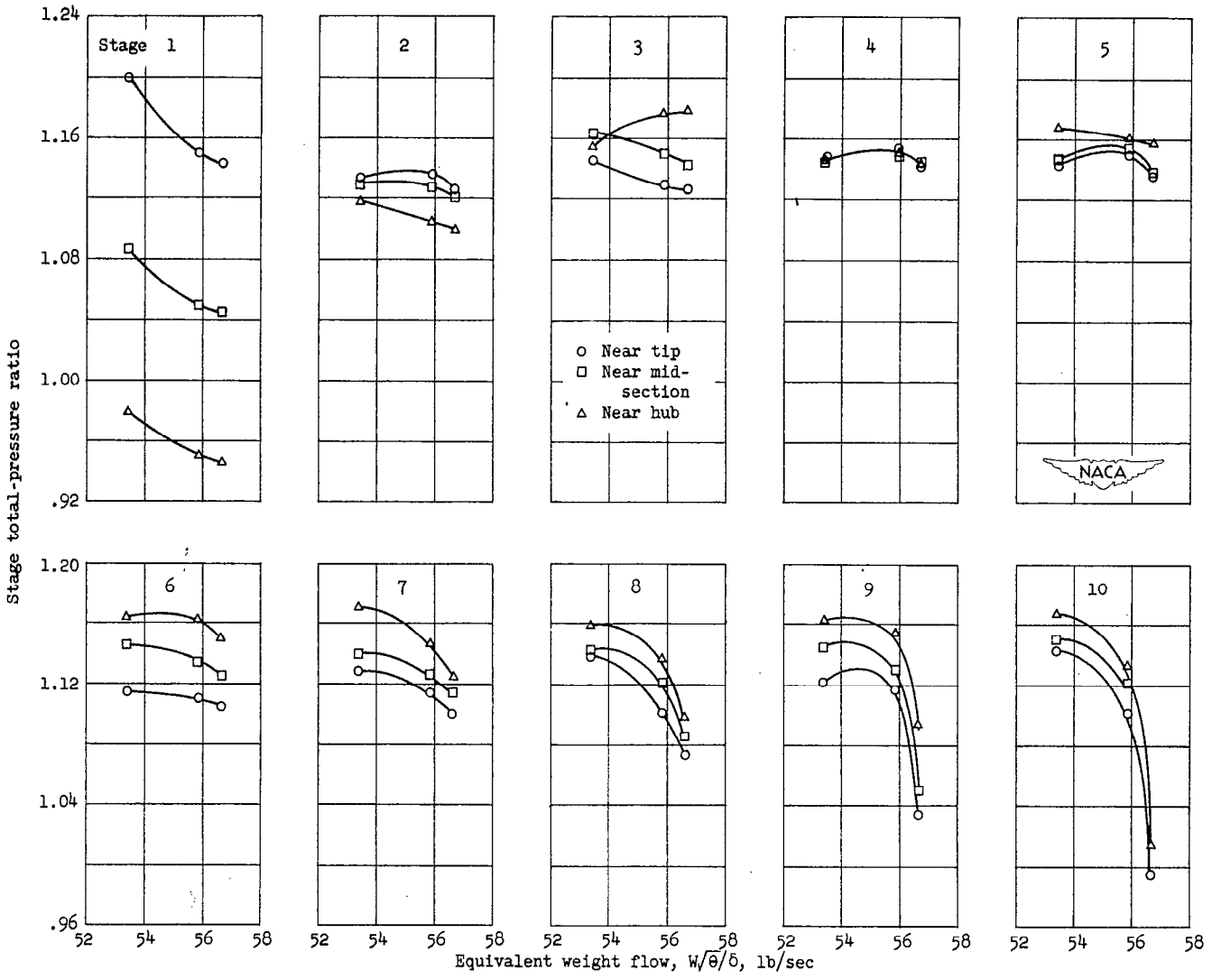

Figure 6. - Variation of stage total-pressure ratio with compressor-inlet equivalent weight flow at three radial measuring stations for all stages.

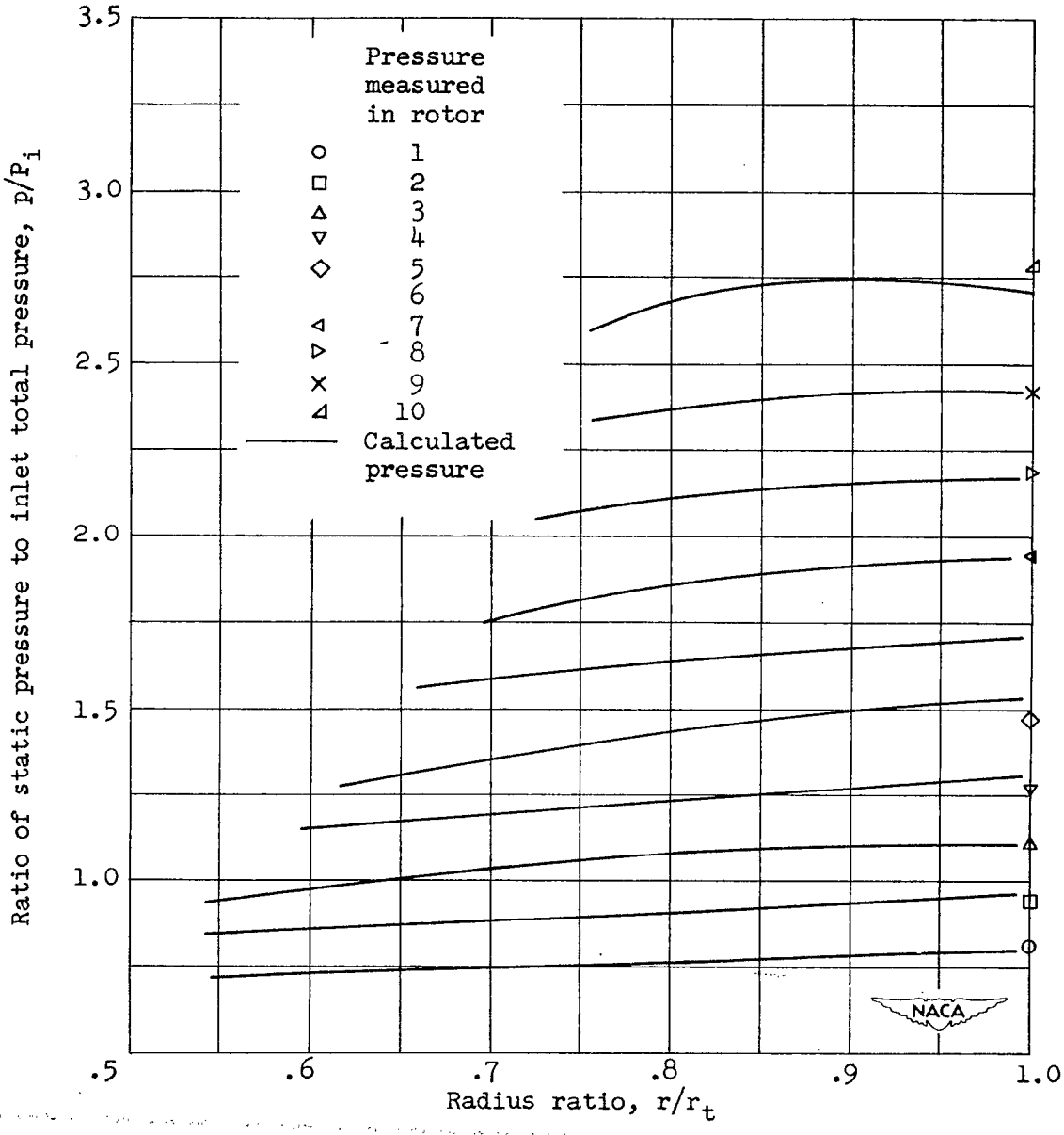

(a) After rotor rows.

Figure 7. - Comparison of calculated static-pressure distribution with measured wall static pressures at peak-efficiency point.

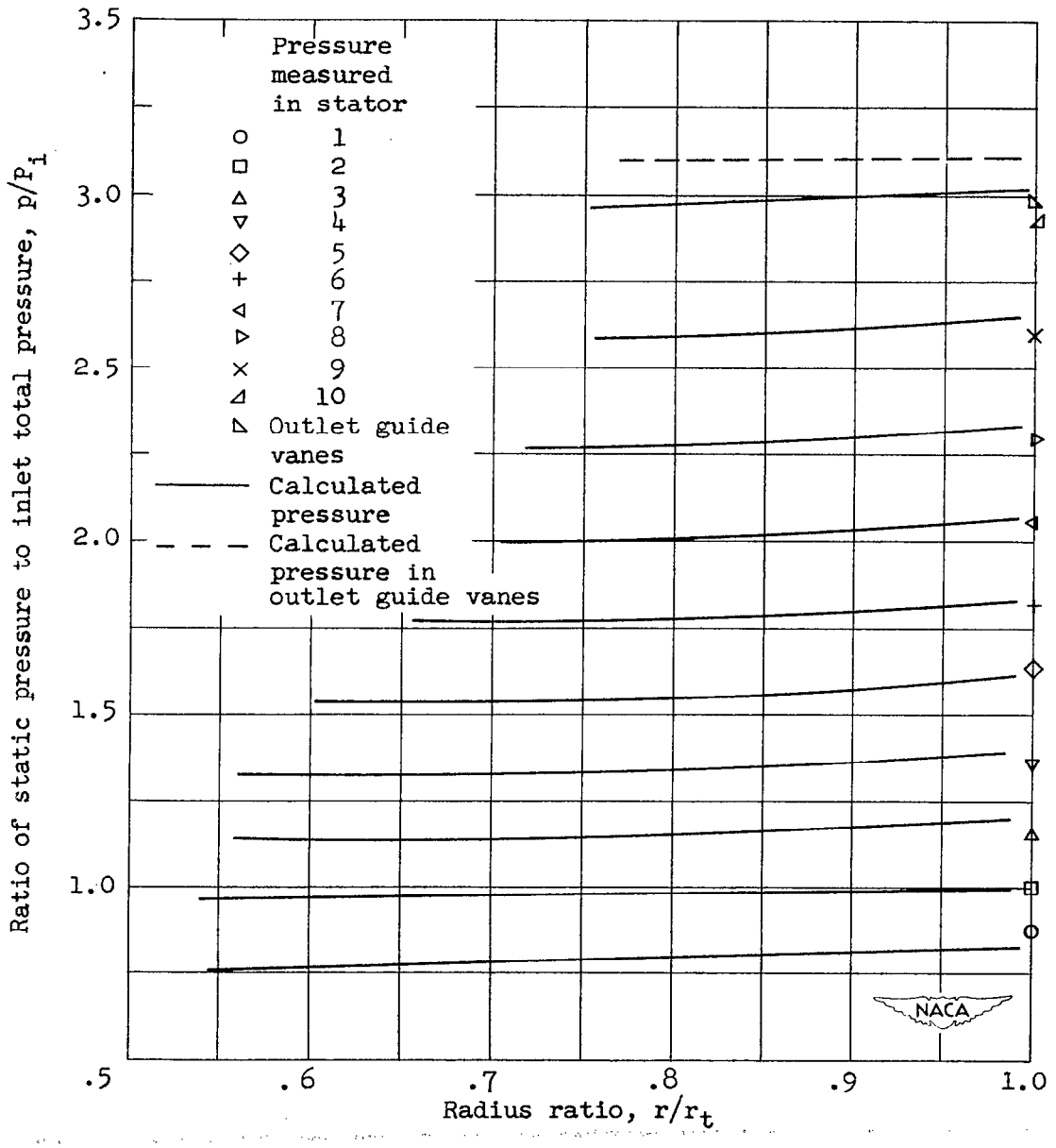

(b) After stator rows.

Figure 7. - Concluded. Comparison of calculated static-pressure distribution with measured wall static pressures at peak-efficiency point.

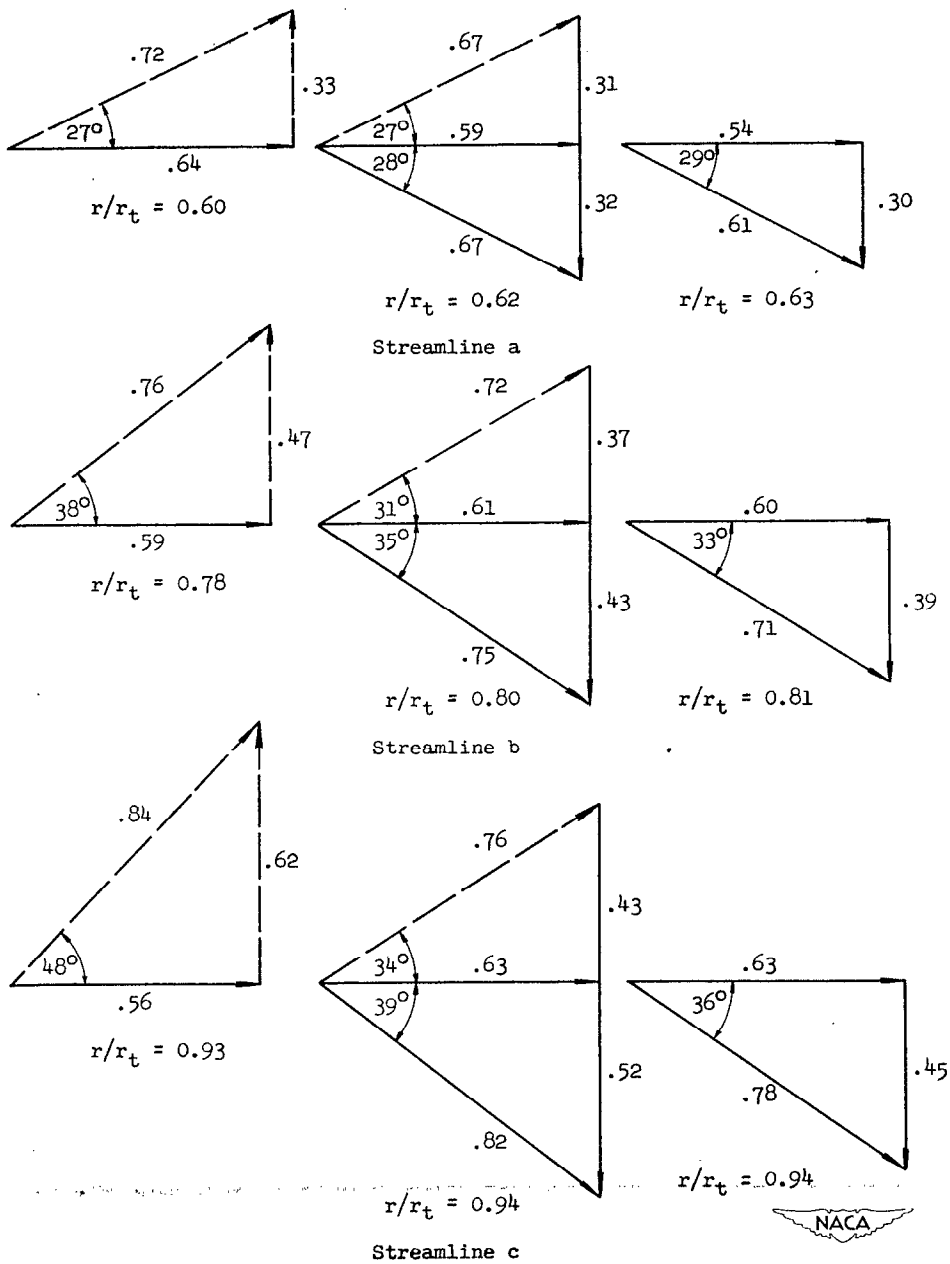

(a) First stage.

Figure 8. - Vector diagrams for all stages at peak-efficiency operating point for the three streamlines determined.

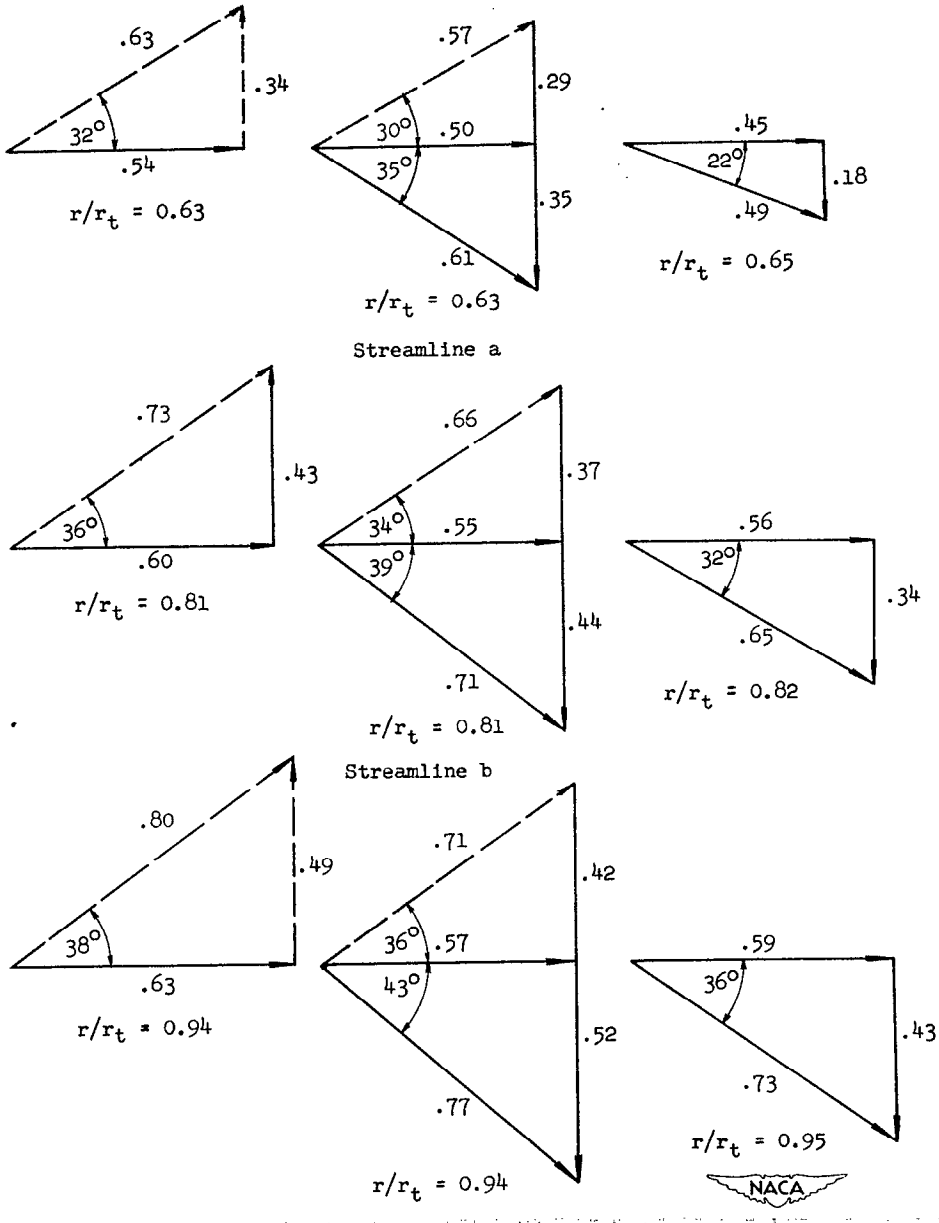

(b) Second stage.

Figure 8. - Continued. Vector diagrams for all stages at peak-efficiency operating point for the three streamlines determined.

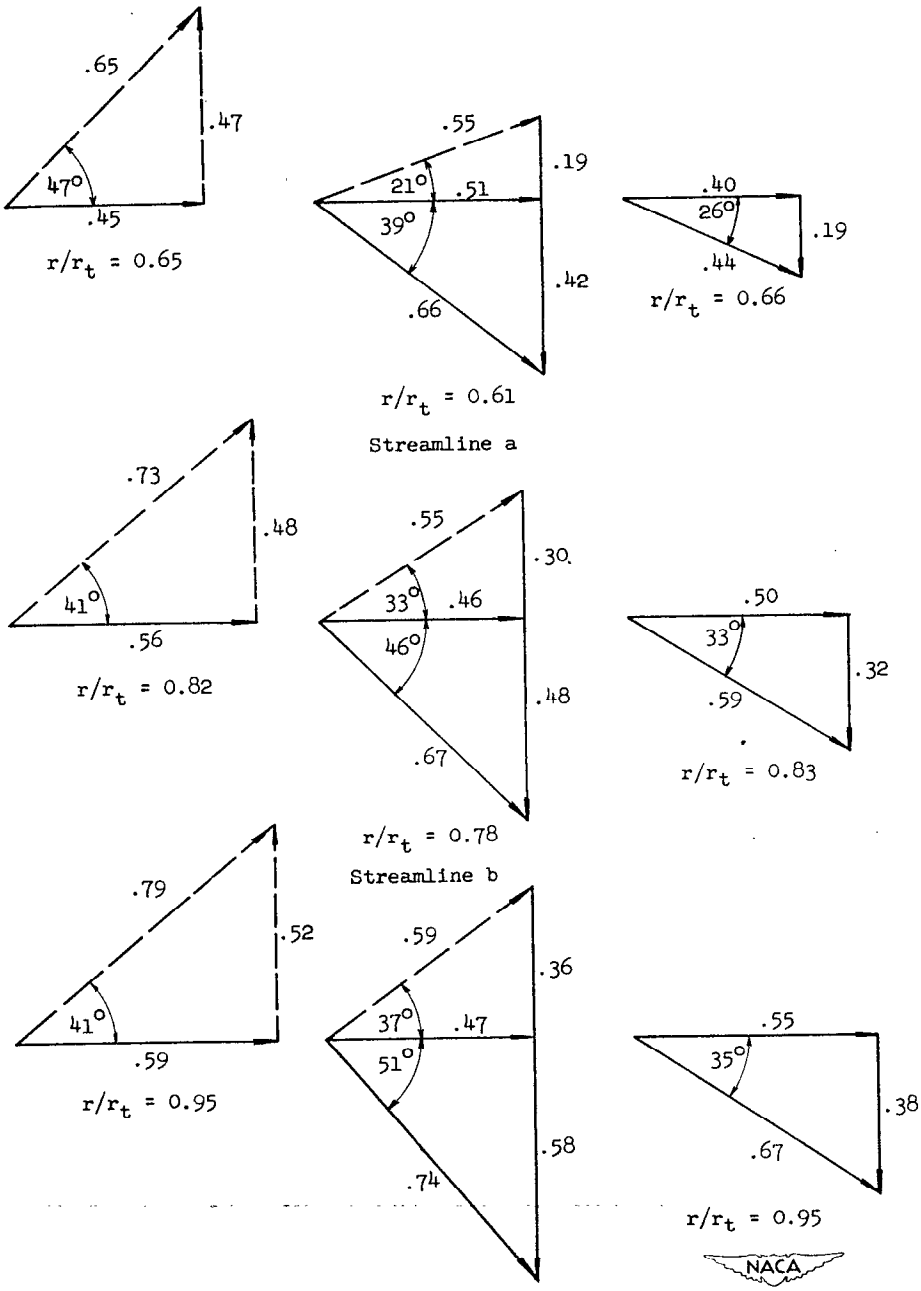

(c) Third stage.

Figure 8. - Continued. Vector diagrams for all stages at peak-efficiency operating point for the three streamlines determined.

[redacted]

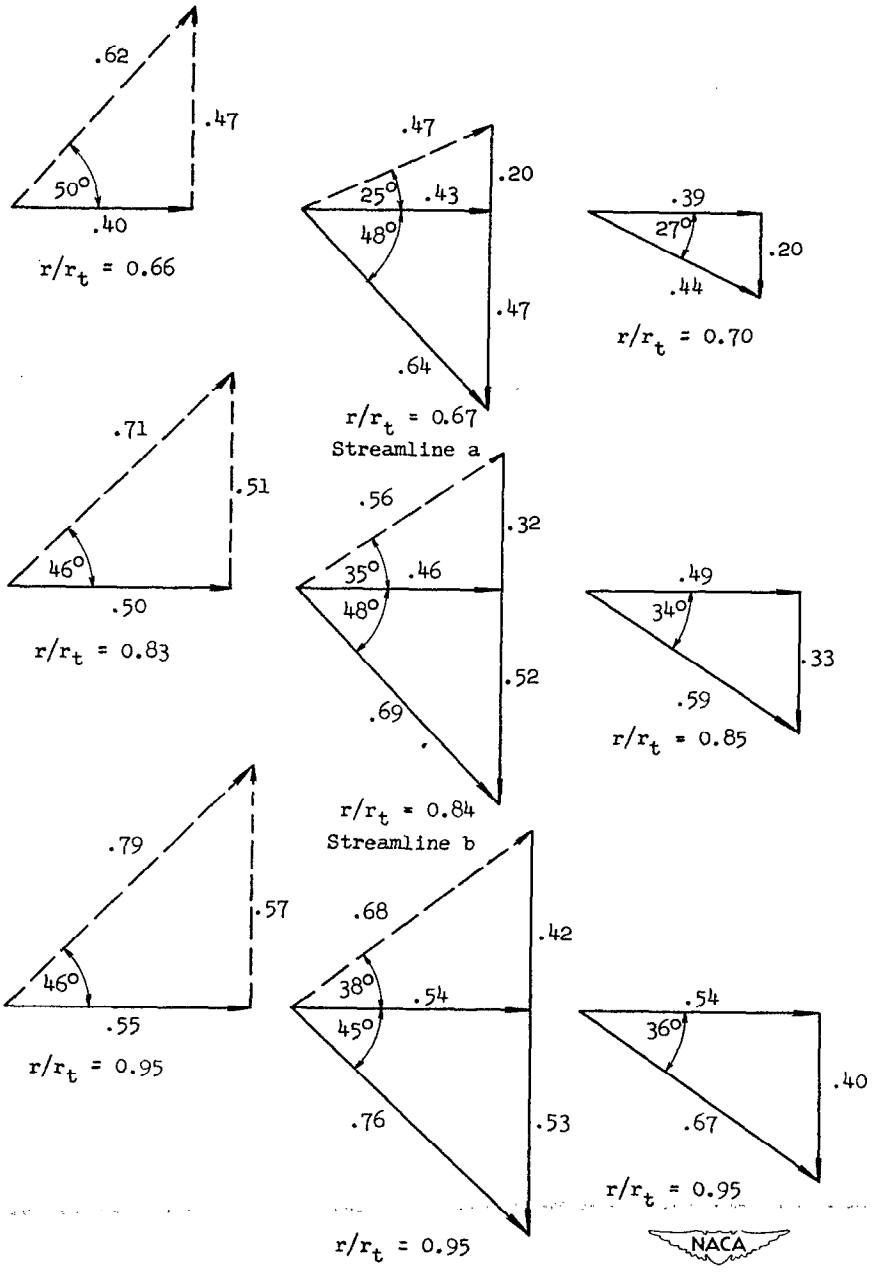

(d) Fourth stage.

Figure 8. - Continued. Vector diagrams for all stages at peak-efficiency operating point for the three streamlines determined.

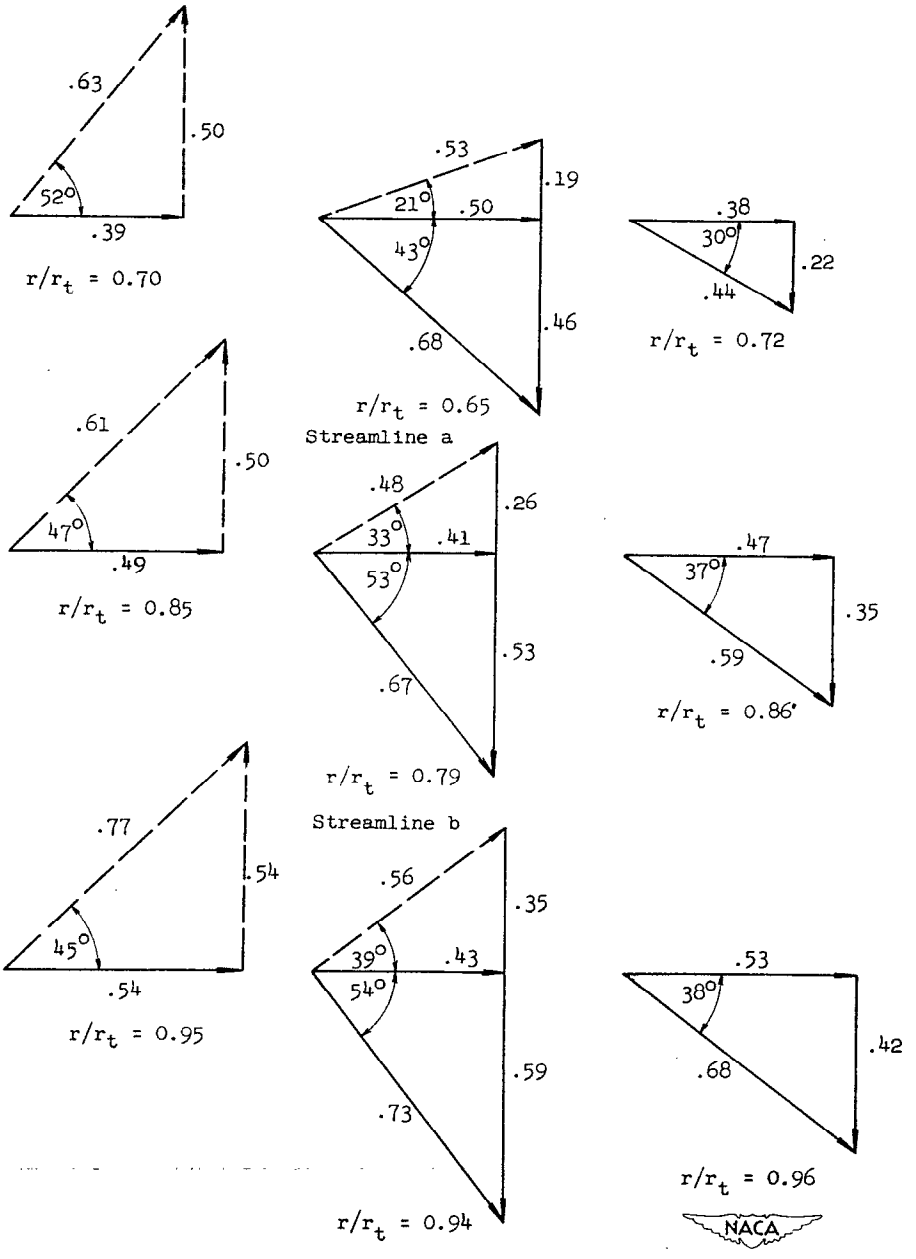

(e) Fifth stage.

Figure 8. - Continued. Vector diagrams for all stages at peak-efficiency operating point for the three streamlines determined.

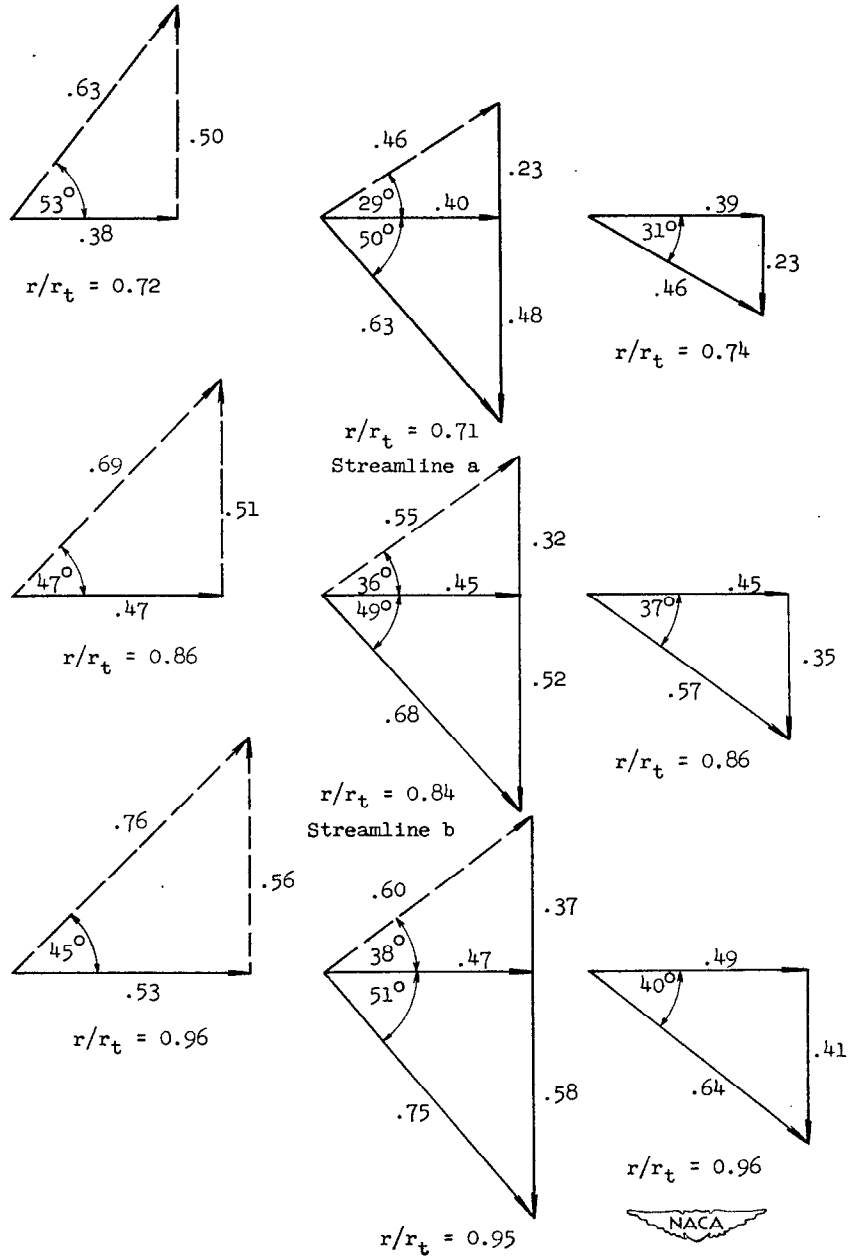

(f) Sixth stage.

Figure 8. - Continued. Vector diagrams for all stages at peak-efficiency operating point for the three streamlines determined.

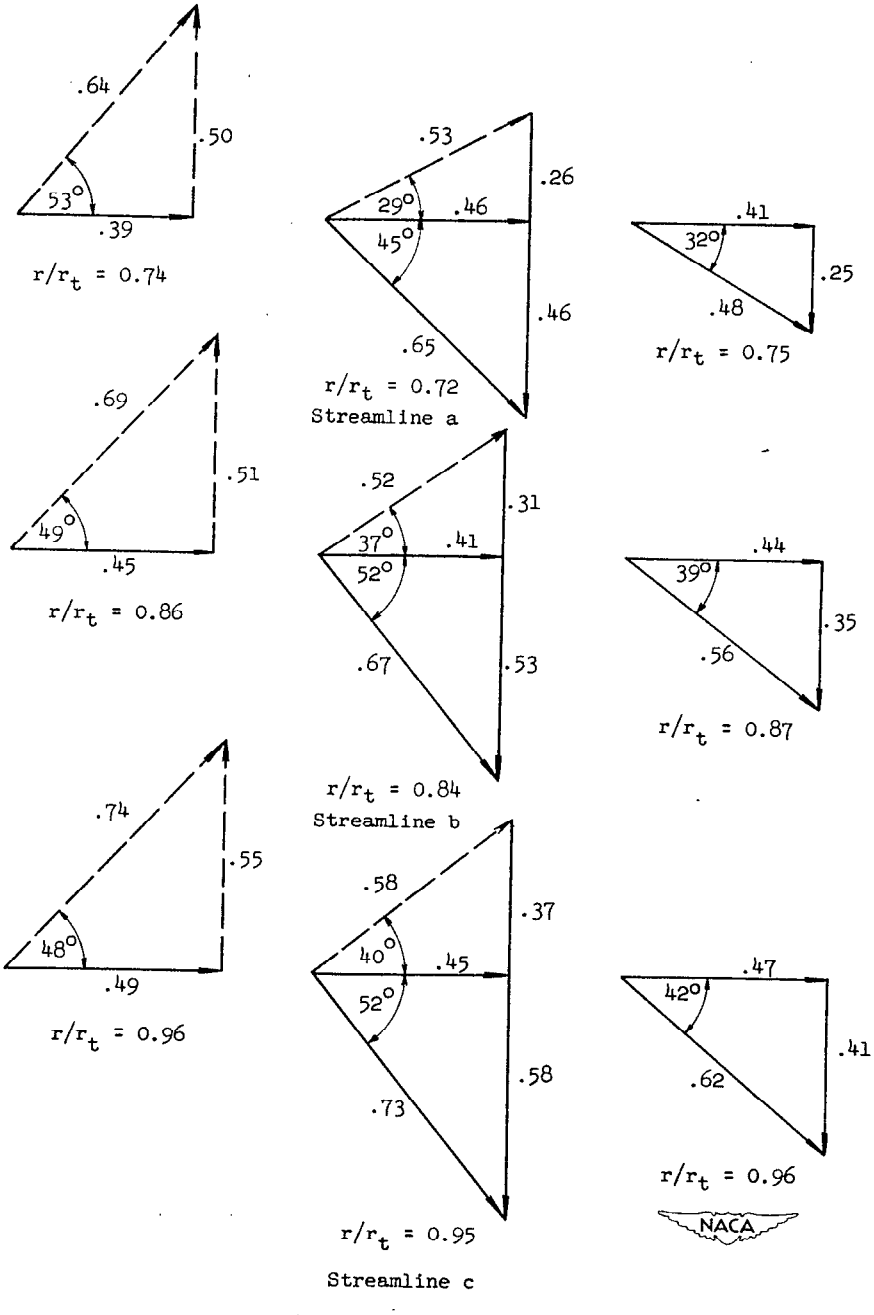

(g) Seventh stage.

Figure 8. - Continued. Vector diagrams for all stages at peak-efficiency operating point for the three streamlines determined.

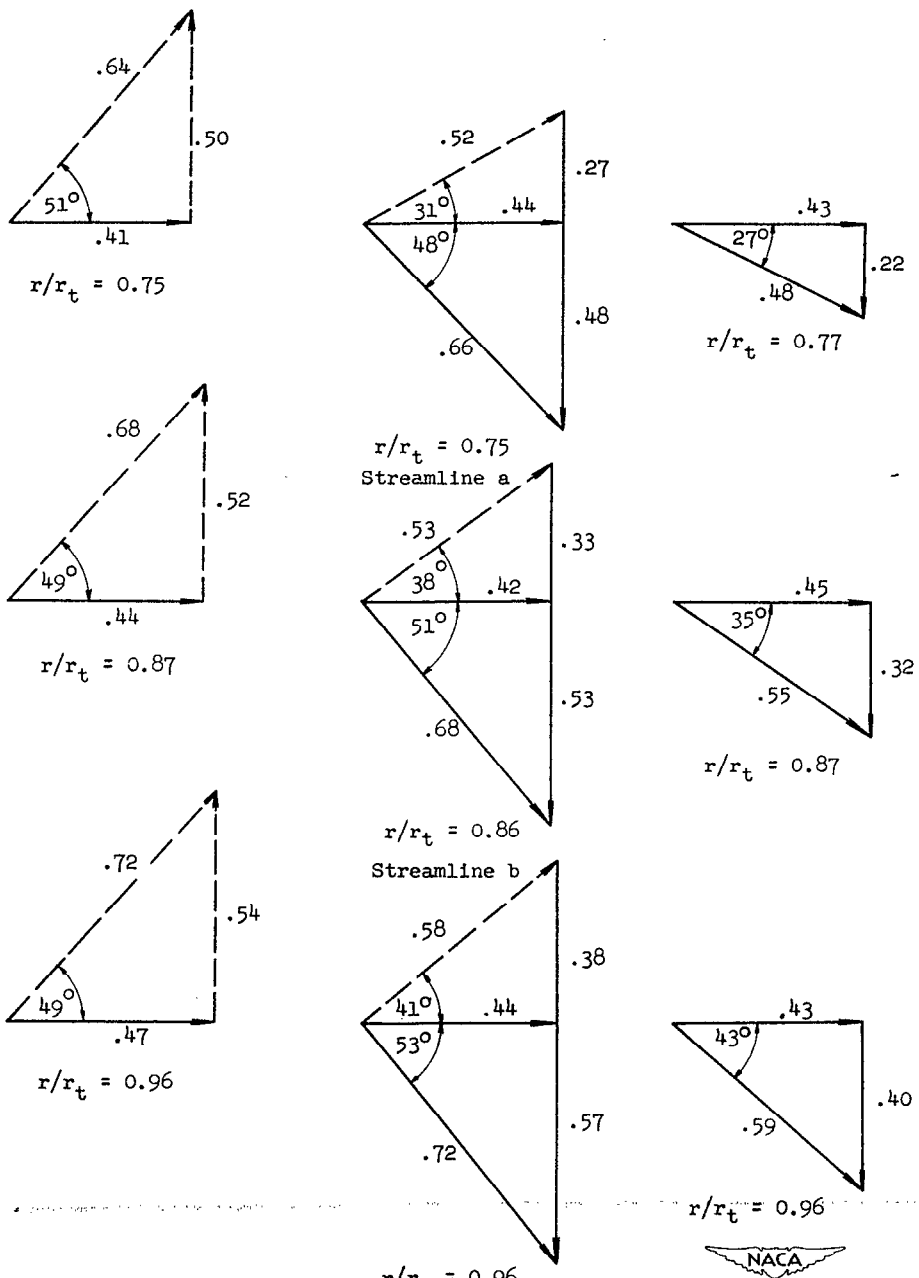

(h) Eighth stage.

Figure 8. - Continued. Vector diagrams for all stages at peak-efficiency operating point for the three streamlines determined.

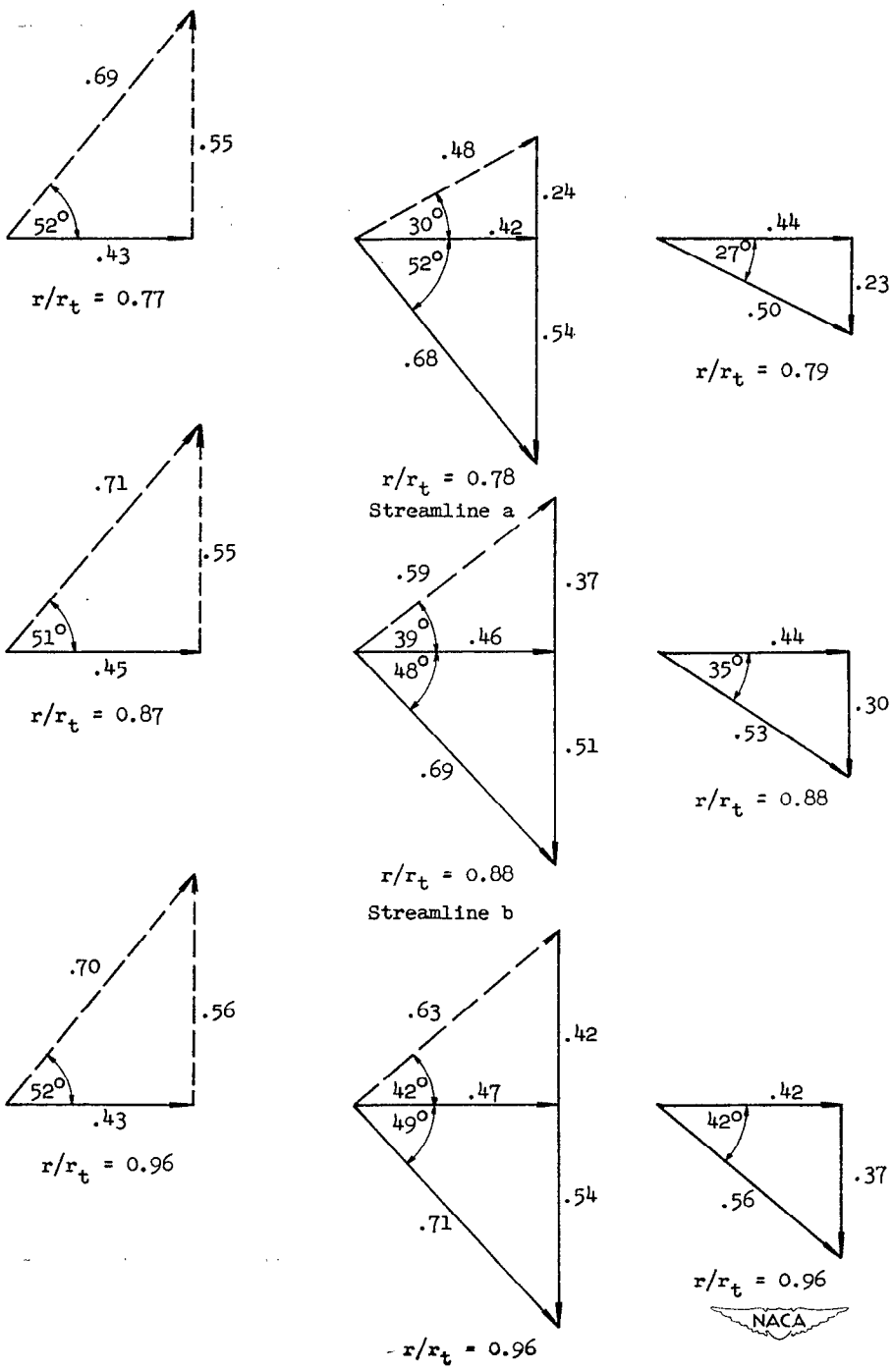

(i) Ninth stage.

Figure 8. - Continued. Vector diagrams for all stages at peak-efficiency operating point for the three streamlines determined.

[redacted]

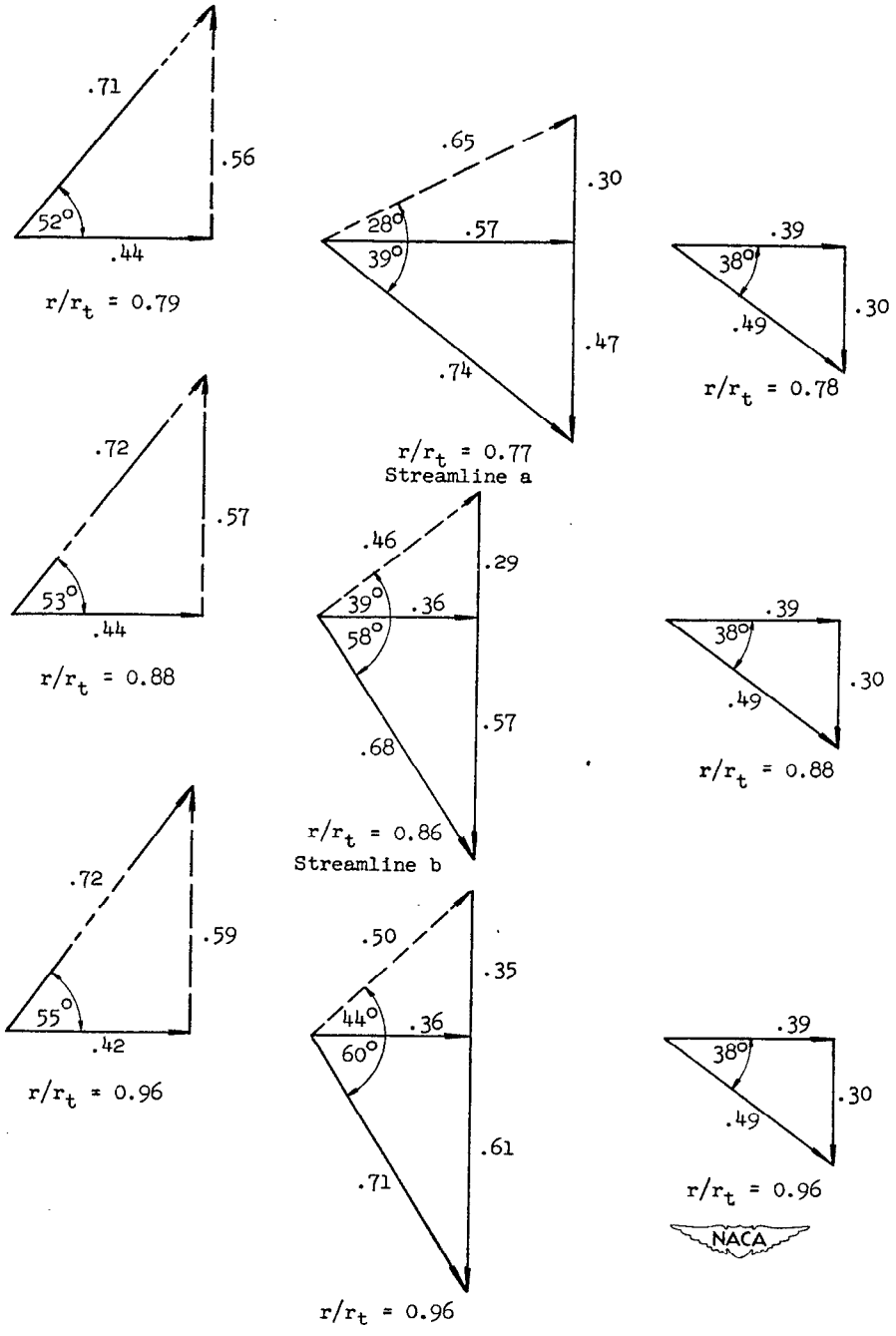

(j) Tenth stage.

Figure 8. - Concluded. Vector diagrams for all stages at peak-efficiency operating point for the three streamlines determined.

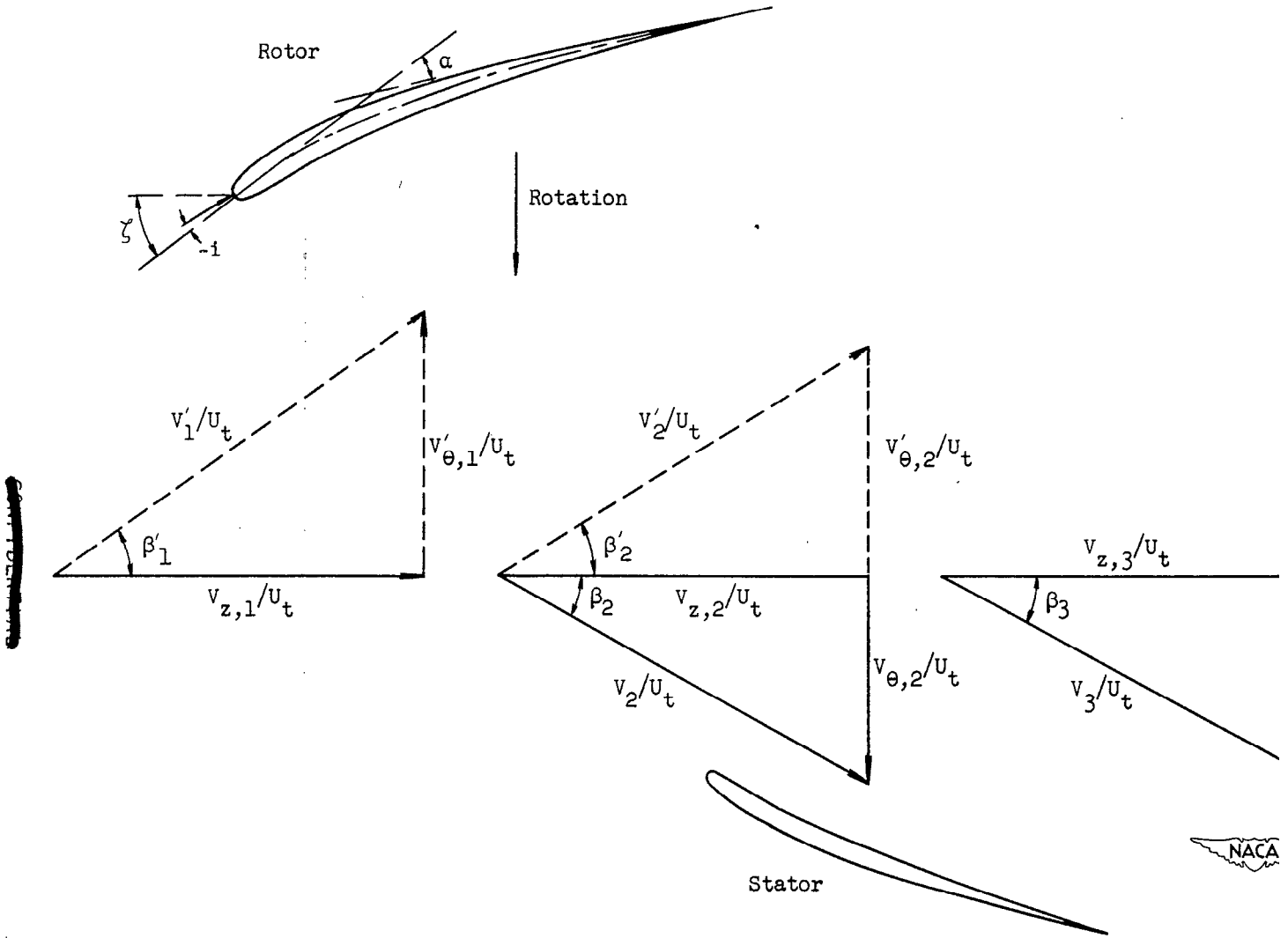

Figure 9. - Velocity-diagram notation.

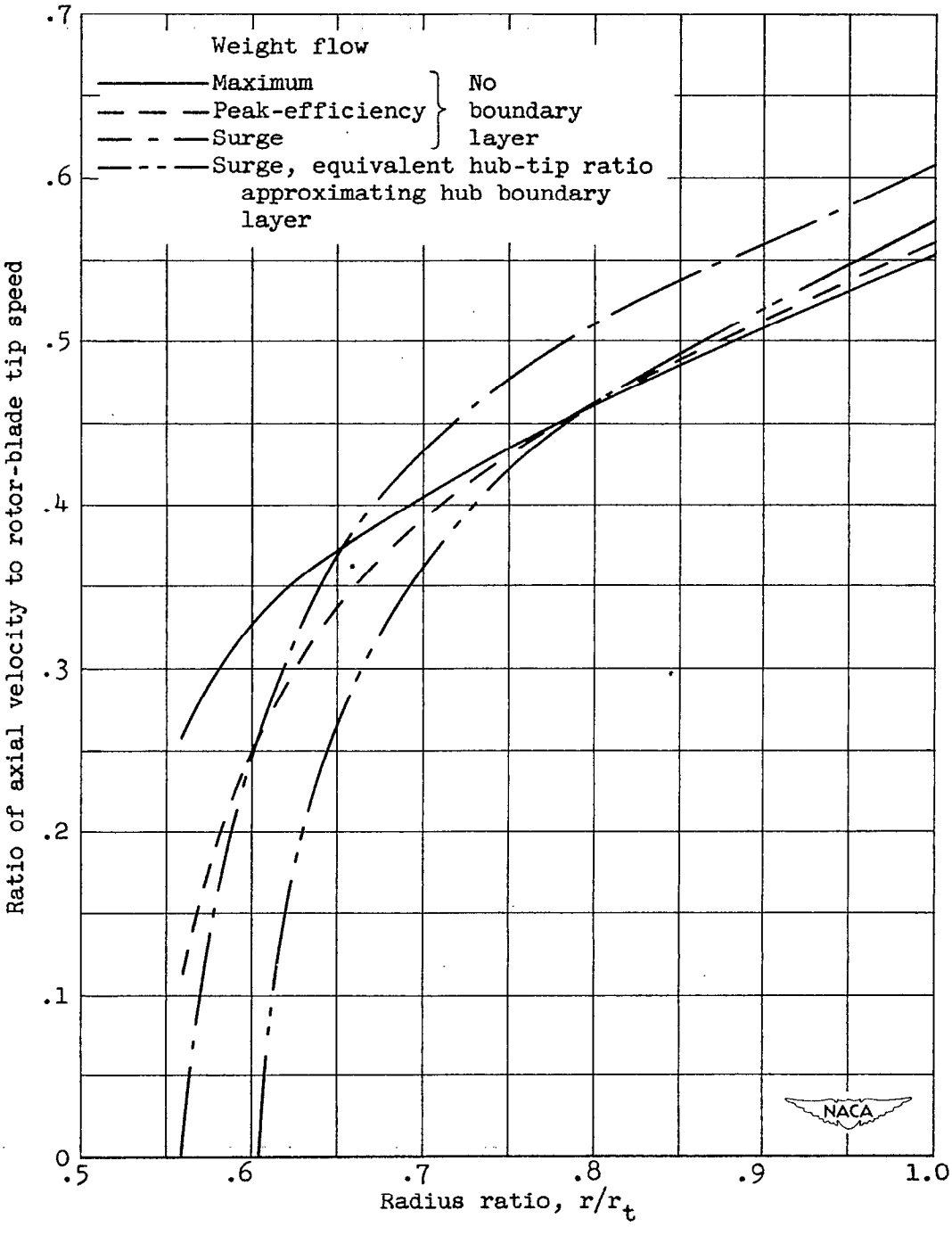

Figure 10. - Radial distribution of axial velocity after fourth stator for various weight flows showing effect of boundary layer at hub at surge.

[redacted]